RMetS
Royal Meteorological Society

A review on Arctic sea-ice predictability and prediction on seasonal to decadal time-scales

Virginie Guemas,[a,b]* Edward Blanchard-Wrigglesworth,[c] Matthieu Chevallier,[b,d] Jonathan J. Day,[e] Michel Déqué,[b] Francisco J. Doblas-Reyes,[a,f] Neven S. Fučkar,[a] Agathe Germe,[b,g] Ed Hawkins,[e] Sarah Keeley,[h] Torben Koenigk,[i] David Salas y Mélia[b] and Steffen Tietsche[e]

[a]*Climate Forecasting Unit, Institut Català de Ciències del Clima (IC3), Barcelona, Spain*
[b]*Centre National de Recherches Météorologiques, Groupe d'Etude de l'Atmosphère Météorologique, Météo-France, UMR3589, Toulouse, France*
[c]*Department of Atmospheric Sciences, University of Washington, Seattle, USA*
[d]*MERCATOR Océan, Toulouse, France*
[e]*NCAS-Climate, Department of Meteorology, University of Reading, UK*
[f]*Institució Catalana de Recerca i Estudis Avançats, Barcelona, Spain*
[g]*Laboratoire d'Océanographie et du Climat, LOCEAN, Paris, France*
[h]*European Center for Medium Range Weather Forecasts, Reading, UK*
[i]*Swedish Meteorological and Hydrological Institute, Norrköping, Sweden*

*Correspondence to: V. Guemas, Institut Català de Ciències del Clima (IC3), Carrer Trueta, 203, 08005 Barcelona, Spain.
E-mail: virginie.guemas@ic3.cat

Sea ice plays a crucial role in the Earth's energy and water budget and has a substantial impact on local and remote atmospheric and oceanic circulations. Predictions of Arctic sea-ice conditions a few months to a few years in advance could be of interest for stakeholders. This article presents a review of the potential sources of Arctic sea-ice predictability on these time-scales. Predictability mainly originates from persistence or advection of sea-ice anomalies, interactions with the ocean and atmosphere and changes in radiative forcing. After estimating the inherent potential predictability limit with state-of-the-art models, current sea-ice forecast systems are described, together with their performance. Finally, some challenges and issues in sea-ice forecasting are presented, along with suggestions for future research priorities.

Key Words: sea ice; Arctic; predictability; perfect model; prediction; initialization; ensembles

Received 7 December 2013; Revised 13 April 2014; Accepted 13 May 2014; Published online in Wiley Online Library

1. Introduction

Sea ice stands as a major component of the climate system through its key impact on the water and energy budgets (e.g. Budyko, 1969). It acts as an insulating cap (e.g. Maykut, 1982), modulating heat, moisture and momentum exchanges between the ocean and the atmosphere, and the amount of absorbed solar radiation at the Earth's surface (Steele *et al.*, 2008). It affects the surface buoyancy flux in North Atlantic deep-water-formation regions (e.g. Dickson *et al.*, 1988) and therefore the Atlantic thermohaline circulation/Atlantic meridional overturning circulation (AMOC; e.g. Holland *et al.*, 2001; Mikolajewicz *et al.*, 2005; Guemas and Salas-Mélia, 2008a).

The rapid decline in sea-ice area (SIA) in the past few decades (Serreze *et al.*, 2007; Stroeve *et al.*, 2012), particularly in summer and autumn, accompanied by a rapid thinning, has been considered as an early indicator of climate change (Walsh, 1983; Solomon *et al.*, 2007; Min *et al.*, 2008; Notz and Marotzke, 2012). The shrinking sea ice also contributes to the polar temperature amplification (Manabe and Stouffer, 1980; Ingram *et al.*, 1989; Serreze *et al.*, 2009; Kumar *et al.*, 2010; Screen and Simmonds, 2010). Furthermore, sensitivity of the atmosphere to extreme sea-ice anomalies (Smith *et al.*, 2003; Chiang *et al.*, 2004; Magnusdottir *et al.*, 2004; Guemas and Salas-Mélia, 2008b) and more realistic anomalies (Alexander *et al.*, 2004; Deser *et al.*, 2007; Guemas *et al.*, 2009; Balmaseda *et al.*, 2010) have been highlighted using general circulation models (GCMs). The rapid sea-ice decline could favour an increase in autumn/winter snowfall over Siberia, northern Canada and Alaska (Deser *et al.*, 2010), snow cover (Deser *et al.*, 2010; Cohen *et al.*, 2012; Liu *et al.*, 2012), a polar stratospheric cooling (Screen *et al.*, 2013), a weakening of the midlatitude jet (Francis *et al.*, 2009; Francis and Vavrus, 2012), and an increase in the frequency of cold Northern Hemisphere midlatitude winter events (Honda *et al.*, 2009; Petoukhov and Semenov, 2010; Cohen *et al.*, 2012; Liu *et al.*, 2012; Yang and Christensen, 2012). These potential impacts of the Arctic sea-ice cover are still debated though.

The societal and economic perspectives of Arctic sea-ice prediction on seasonal to decadal time-scales have led to increasing efforts in the development of sea-ice forecast systems (Eicken, 2013). Advanced knowledge about the potential opening of maritime routes such as the Northern Sea route (north of

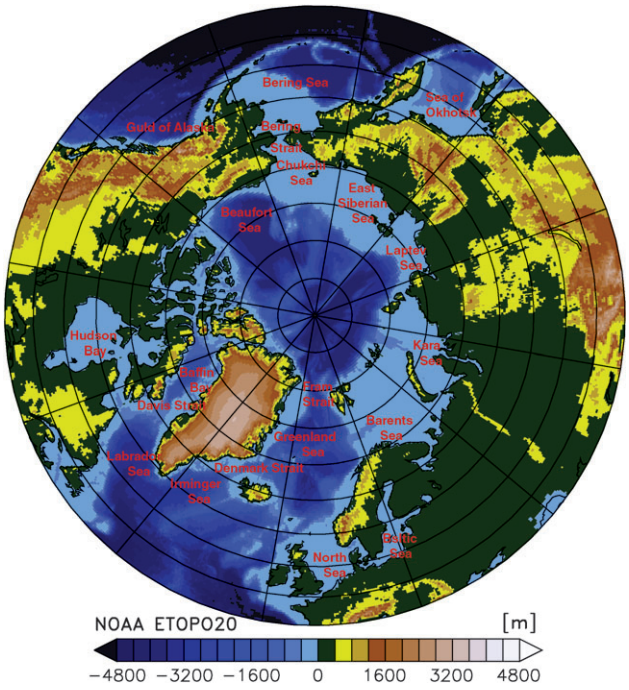

Figure 1. Map of the Arctic seas and straits mentioned in this article. The topography, with a 20 min resolution, was obtained from the National Geophysical Data Center from the National Oceanic and Atmospheric Administration (NOAA).

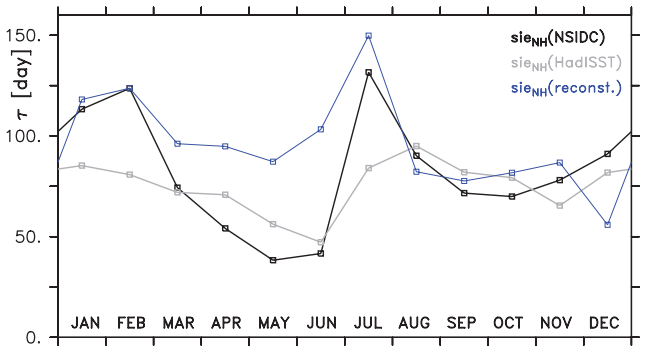

Figure 2. E-folding time-scale of the correlation between the monthly linearly detrended Arctic sea-ice-extent anomalies and the monthly linearly detrended sea-ice-extent anomalies of the following month from the NSIDC observational dataset (Fetterer *et al.*, 2002) in black, the HadISST dataset (Rayner *et al.*, 2003) in grey and the HistDfsNudg sea-ice reconstruction from Guemas *et al.* (2014) in blue.

Russia) and the Northwest Passage (through northern Canada) could offer faster and cheaper shipping between the Atlantic and Pacific Oceans (Hassol, 2004; Smith and Stephenson, 2013). Information on the marine accessibility of Arctic seas and the duration of the ice-free season in the marginal ice zone (MIZ) would allow planning of the exploitation of resources, ship supplies and fishing and hunting activities, which are of particular interest for the Inuit populations. The growing polar ecotourism industry could also benefit from sea-ice predictions.

In this article, we review the key scientific results that triggered the development of operational seasonal-to-decadal predictions of Arctic sea-ice conditions and the history of those developments. Section 2 presents an overview of the mechanisms that suggest a predictability of the sea-ice conditions from a few months to a few years in advance. Section 3 summarizes the results from pseudo-predictions, initialized from a reference simulation with a small perturbation. This approach provides an upper bound on the predictive capability of state-of-the-art climate models, given the current knowledge of sea-ice processes. Section 4 presents the current forecast systems, their initialization and performance. Section 5 provides a discussion of future research priorities. An appendix describes all the coupled climate models and sea-ice models mentioned in the article. Figure 1 shows the location of the seas and straits referred to in this article.

2. Predictability mechanisms for the Arctic sea-ice cover

2.1. *Persistence*

Persistence of sea-ice anomalies stands as the first source of predictability for those same ice anomalies. Based on gridded *in situ* observations covering the 1953–1977 period, Walsh and Johnson (1979) extracted the main modes of variability in Arctic SIA (computed as eigenvectors) and obtained an autocorrelation larger than 0.2 up to a 3 month lag for each mode, without specifying if this persistence varies throughout the year. From weekly observations covering the 1979–2004 period, Lukovich and Barber (2007) obtained coherent sea-ice concentration (SIC) persistence patterns with time-scales of 3–7 weeks, with a maximum in late summer and early autumn and in the Kara, Beaufort and Chukchi Seas. In the National Snow and Ice Data Center (NSIDC) observations (Fetterer *et al.*, 2002) from 1978 to 2008, Blanchard-Wrigglesworth *et al.* (2011a) obtained a characteristic e-folding time-scale for the total Arctic SIA that varies seasonally from 2 to 5 months. E-folding time-scales of 2–5 months have also been identified in different climate models (Day *et al.*, 2014) such as the Community Climate System Model version 3 (CCSM3, Blanchard-Wrigglesworth *et al.*, 2011a), the Centre National de Recherches Météorologiques (CNRM) Coupled Model version 3.3 (CNRM-CM3.3, Chevallier and Salas-Mélia, 2012), the Hadley Centre Global Environment Model version 1.2 (HadGEM1.2), the Geophysical Fluid Dynamics Laboratory Coupled Model version 3 (GFDL-CM3), the EC-Earth (European Consortium Earth) 2.3 model and the Max Planck Institute for Meteorology's Earth-System Model (MPI-ESM). Longer persistence is seen in winter and summer than the other seasons (Figure 2), but whether winter or summer persistence is larger is model dependent (Day *et al.*, 2014). The September SIA (month of the annual minimum) is significantly correlated with only the previous July and August SIA, according to Blanchard-Wrigglesworth *et al.* (2011a). Blanchard-Wrigglesworth *et al.* (2011a) also illustrated the significant negative correlation between the absolute value of the climatological rate of ice-edge retreat/advance as a function of the calendar month and the persistence time-scale as a function of the calendar month (also found by Day *et al.*, 2014). Those results were confirmed by Chevallier and Salas-Mélia (2012) with a different diagnostic: the 1-month squared lagged-anomaly correlation (SLAC), which provides the amount of variance explained by the persistence only, is maximum for pairs of months between which the SIA varies the least.

The persistence of sea-ice thickness (SIT, Figure 3) and sea-ice volume (SIV) is much longer than the persistence of SIC and SIA. Blanchard-Wrigglesworth *et al.* (2011a) estimated the persistence time-scale of SIT as approximately 1 year in the central Arctic and a few months in the seasonal ice zone. Advective processes might be responsible for the considerably shorter persistence time-scale at the regional scale. Indeed, the total Arctic SIV has a persistence time-scale estimated to be between 4 (Blanchard-Wrigglesworth, 2011a) and 10 (L'Hévéder and Houssais, 2001) years. Seasonal variations in the SIV e-folding time-scales were highlighted by Day *et al.* (2014), with a minimum found between May and July, which suggests a potentially lower skill in seasonal forecasts of the SIV in summer than in any other season. Under a climate change scenario, Blanchard-Wrigglesworth *et al.* (2011a) obtained a strong decline in persistence of the Arctic SIV, which was related to the ice thinning.

2.2. *Advection*

The advection of sea-ice anomalies by the mean Arctic circulation can provide additional predictability over simple persistence, especially for local quantities such as SIC or SIT. The impact

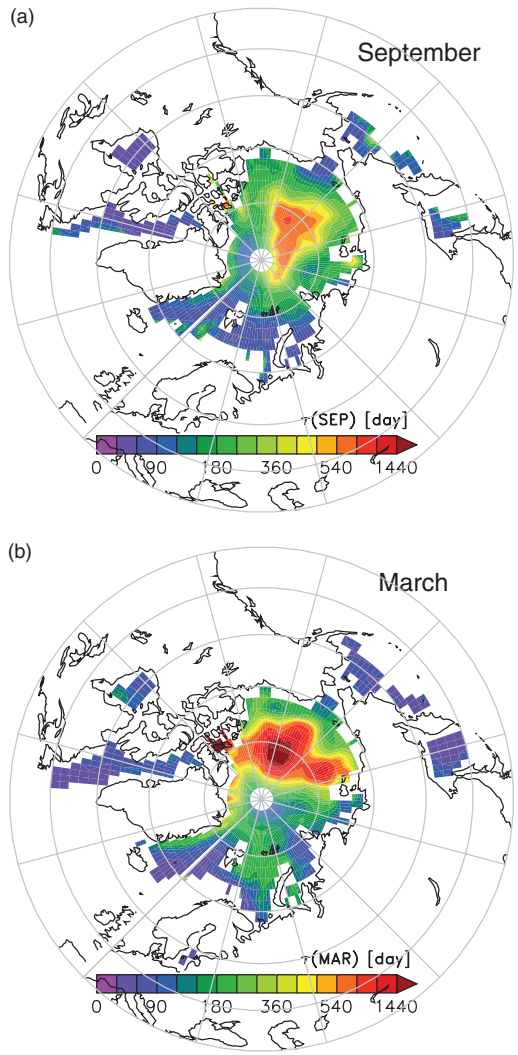

Figure 3. E-folding time-scale of the correlation between the (a) September or (b) March linearly detrended sea-ice-thickness anomalies and the monthly linearly detrended sea-ice-thickness anomalies of the following month from the HistDfsNudg sea-ice reconstruction from Guemas *et al.* (2014).

on integrated quantities such as SIA or SIV is indirect, through the interaction with the other climate components (e.g. warmer conditions). The mean Arctic sea-ice circulation (Gordienko, 1958) is characterized by an anticyclonic gyre in the Beaufort Sea and a cyclonic gyre of smaller extent in the Laptev Sea. At their frontier appears the Transpolar Drift Stream, originating in the Chukchi Sea and exiting the Arctic Ocean through Fram Strait. Gudkovich (1961a, 1961b) described two types of circulation. In the anticyclonic regime, the area of the Beaufort gyre increases and the area of the Laptev gyre shrinks; the Transpolar Drift Stream originates from the Laptev, East Siberian and Chukchi Seas and transports ice toward the Greenland Sea (Figure 4(a)). In the cyclonic regime, a contraction of the Beaufort gyre occurs simultaneously with an expansion of the Laptev gyre; the Transpolar Drift Stream slows down and its entrance shifts toward the Beaufort Sea (Figure 4(b)). The cyclonic regime is associated with a larger sea-ice export through Fram Strait because the exported ice is thicker than in the anticyclonic regime (Polyakov *et al.*, 1999). Karklin (1977) suggested a periodicity of 6–7 years in the ice drift, confirmed by Proshutinsky and Johnson (1997), who observed shifts between the anticyclonic and cyclonic regimes every 5–7 years. If predictable, those circulation regimes would provide predictability in the sea-ice conditions on decadal time-scales.

The SIT anomalies formed in the Beaufort gyre and along the Siberian coast propagate in the Transpolar Drift Stream and are transported southward through Fram Strait, where they melt and enter the Labrador Sea as a freshwater anomaly about 2 years after

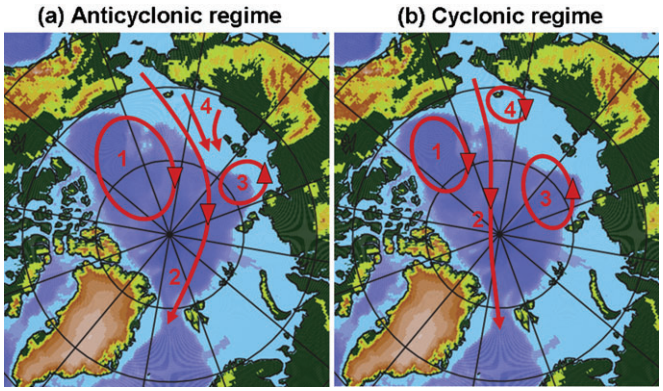

Figure 4. (a) Anticyclonic and (b) cyclonic regimes of surface Arctic circulation, simplified from Sokolov (1962): 1, Beaufort gyre; 2, Transpolar Drift Stream; 3, Laptev sea gyre; 4, East Siberian circulation.

crossing Fram Strait. Large ice exports were very likely responsible for the formation of the so-called Great Salinity Anomalies in the Labrador Sea and strongly reduced the deep-water formation in the Labrador Sea (e.g. Dickson *et al.*, 1988; Belkin *et al.*, 1998; Häkkinen, 1999; Haak *et al.*, 2003; Koenigk *et al.*, 2006). Such reduced convection prevented relatively warm water from the deeper Labrador Sea coming to the surface. Together with an increase in the freezing point due to the freshwater anomaly, this favoured sea-ice formation. Observational data (Venegas and Mysak, 2000) also suggested that Fram Strait sea-ice export drives a substantial part of the ice-cover variability in the Greenland Sea on interannual time-scales. These mechanisms could provide predictability of the sea-ice conditions in the Atlantic MIZ.

2.3. *Atmosphere*

The atmosphere plays a major role in driving Arctic sea-ice variability. The atmospheric circulation, if predictable, can therefore contribute to the predictability of the sea-ice conditions. Using a hydraulic model forced by winds and Atlantic water inflow, Gudkovich (1961a, 1961b) concluded that the subseasonal to interannual variability in the Arctic surface circulation was primarily wind driven. This was later confirmed by a series of studies using two-dimensional numerical models (e.g. Proshutinsky, 1988, 1993; Proshuntinsky and Johnson, 1997), and three-dimensional coupled ice–ocean models (e.g. Walsh and Chapman, 1990; Serreze *et al.*, 1992; Mysak and Venegas, 1998). According to Gudkovich (1961a, 1961b), the anticyclonic ice-circulation regime usually occurs under a prominent polar high centred over the Beaufort Sea. The cyclonic regime, however, prevails under the dissipation of such a polar high and the northern extension of the Siberian High, together with a strengthening and an extension of the Icelandic Low towards Baffin Bay and the Kara Sea (Johnson *et al.*, 1999). Using the two-dimensional barotropic dynamic sea-ice model from Proshutinsky and Jonhson (1997), Johnson *et al.* (1999) showed that the transition to the cyclonic (anticyclonic) regime is associated with a fall (rise) of 5–8 hPa in sea-level pressure (SLP) over the central Arctic, a rise (fall) by 2–4 hPa in the Greenland High, a weakening (strengthening) of the Aleutian Low and a strengthening (weakening) of the Azores High.

The North Atlantic Oscillation (NAO)–Arctic Oscillation (AO) has been suggested to substantially affect the sea-ice velocities and subsequent transports in the Arctic region (e.g. Mysak and Venegas, 1998; Kwok, 2000; Rigor *et al.*, 2002; Krahmann and Visbeck, 2003; Zhang *et al.*, 2004), with exchanges of sea ice between the Siberian Arctic and the North American Arctic (e.g. Rigor *et al.*, 2002; Zhang *et al.*, 2004). Observational data from the 1979 to 1998 period indicated that a winter (January–March) positive AO favours the advection of ice away from the Siberian coast, longer recirculations of ice within the Beaufort gyre and an

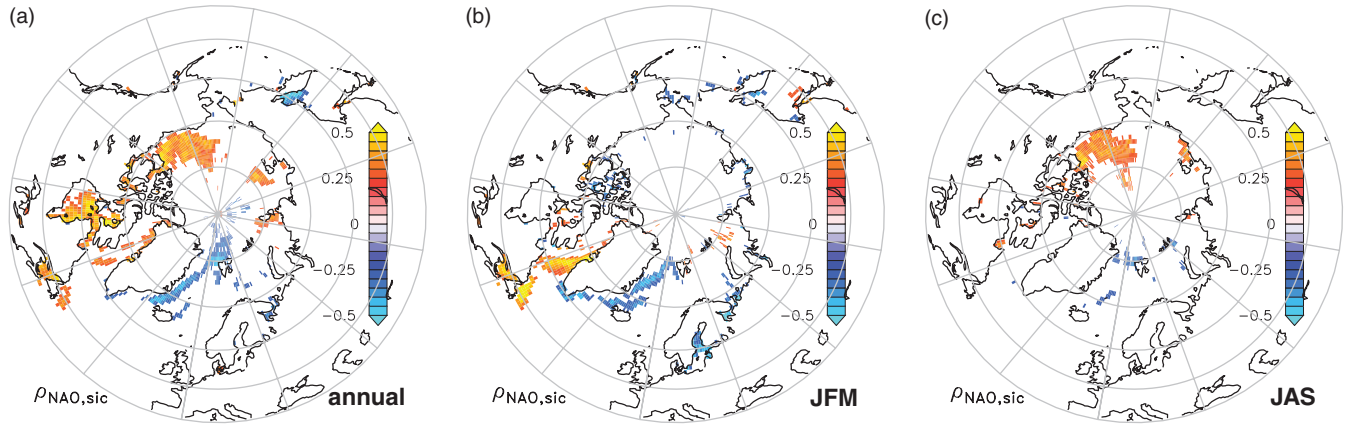

Figure 5. Correlation over the 1958–2013 period between the linearly detrended observed (a) annual mean, (b) winter mean (January–March) and (c) summer mean (July–September) North Atlantic Oscillation (NAO) index (http://www.cpc.ncep.noaa.gov) and the linearly detrended (a) annual mean, (b) winter mean and (c) summer mean SIC from HadISST. Only the regions where the correlation is significant to the 95% level using a two-tailed Student's t test are shown.

increase in the export of thinner ice through Fram Strait (Rigor *et al.* 2002).

Observational data (Venegas and Mysak, 2000; Kwok *et al.*, 2013) and model analyses (Döscher *et al.*, 2010) suggested a dominant role of the wind variability on the Fram Strait sea-ice export, 80% of its variance being explained by the SLP gradient across the Fram Strait during winter and spring based on satellite data (Kwok and Rothrock, 1999; Ogi *et al.*, 2010). A significant correlation of the Fram Strait sea-ice export with the NAO during the winter season (defined as December–March) was obtained from satellite data (Kwok and Rothrock, 1999; Kwok, 2009), which has since been shown to be non-stationary (Hilmer and Jung, 2000; Vinje, 2001b: Holland, 2003; Schmith and Hansen, 2003). Using observational data from 1979 to 1998, Wu *et al.* (2006) instead suggested a dominant role of the Arctic Dipole Anomaly (DA) on the variability of the Fram Strait sea-ice export. The DA is characterized by a SLP dipole with centres located over the Kara and Laptev Seas and over the Canadian Archipelago. Tsukernik *et al.* (2009) highlighted a similar SLP dipole but with centres located over the Barents Sea and Greenland, using observational data from 1979 to 2006. The variability in sea-ice drift and Fram Strait sea-ice export is, to a large extent, driven by SLP variability. As our ability to predict the latter beyond 1–2 weeks is currently very low, those mechanisms do not provide significant sources of sea-ice predictability.

The NAO is thought to drive a seesaw in sea-ice conditions between the Labrador Sea and the Greenland and Barents Seas (Figure 5). The SIA in the former (latter) is positively (negatively) correlated with the NAO index (e.g. Walsh and Johnson, 1979; Deser *et al.*, 2000; Vinje, 2001a), with a maximum correlation at a lag of about 2 weeks in the sea-ice response to the NAO (Fang and Wallace, 1994) and a significant correlation until a lag of 2 years (Partington *et al.*, 2003; Ukita *et al.*, 2007). Observational data (1903–1994) indicated that the SIA in the Labrador Sea is mainly driven by the thermodynamic effects related to the local wind forcing (Venegas and Mysak, 2000). Model analyses also suggested that a positive winter NAO could reduce summer SIT in the Kara, Laptev, East Siberian and Chukchi Seas and in Baffin Bay (Döscher *et al.*, 2010). Furthermore, observational data suggested that a positive NAO could favour positive SIC anomalies in the Beaufort Sea (Mysak and Venegas, 1998; Arfeuille *et al.*, 2000). In the Pacific Sector, a SLP dipole between the East Siberian and Bering Seas would drive a seesaw in sea-ice conditions between the Bering Sea and the Sea of Okhotsk through wind stress and local thermodynamic effects, according to observational data from the 1972 to 1989 period (Fang and Wallace, 1994).

Anomalies in sea-ice cover could feed back onto the large-scale atmospheric circulation and could provide memory on seasonal to decadal time-scales through coupled ice–atmosphere or ice–ocean–atmosphere mechanisms (Mysak and Venegas, 1998; Goosse *et al.*, 2002, 2003; Bengtsson *et al.*, 2004). However, the impact of SIC anomalies on the atmosphere does not appear to be large enough to provide the potential for such a feedback loop (e.g. Alexander *et al.*, 2004; Magnusdottir *et al.*, 2004). Although the atmosphere stands as a major driver of the Arctic sea-ice conditions, its low predictability beyond 1 or 2 weeks make the mechanisms presented in this section 'sinks', rather than sources, of sea-ice predictability.

2.4. *Ocean*

The long memory of the ocean makes it a major source of climate predictability (e.g Griffies and Bryan, 1997; Boer, 2004). The ocean can act as a source of sea-ice predictability, dynamically through its drag effect on the ice motion and thermodynamically through basal heat exchanges. Bitz *et al.* (2005) assessed the main factors controlling the location of the ice edge among advection, deformation, atmospheric and oceanic heat fluxes in a 1000-year present-day simulation (under 1990 greenhouse gas concentrations) and a climate projection. They illustrated the key role of ocean heat-flux convergence in determining the location of the winter sea-ice edge through the basal melt, which dominates the SIV budget. The long persistence time-scales in the ocean allow for a winter-to-winter memory of the location of the ice edge in the MIZ. The sea-ice edge stands at the location of ocean thermal fronts in the Nordic Seas (Wadhams, 1981).

In the Atlantic Sector, the ocean heat transport via the North Atlantic Current was highlighted three decades ago as a chief cause of the sea-ice melting in numerical studies (Hibler, 1986; Hibler and Bryan, 1987; Semtner, 1987). The SALARGOS buoy during October 1988 registered a strong upward heat flux in the North Atlantic sector contributing to sea-ice melting (Steele and Morison, 1993), favoured by a lack of strong permanent halocline in those regions (Rudels *et al.*, 1996). Based on observational data covering the 1903–1994 period, Venegas and Mysak (2000) suggested that the variability of the sea-ice cover in the Barents Sea would be mainly driven by the temperature and the strength of the Norwegian Currents on interannual time-scales. Also based on observations of the 1864–1998 period, Vinje (2001a) highlighted a strong link between the Atlantic water temperatures in the southern Norwegian Sea and the sea-ice extent (SIE) 2–3 years later in the Barents and Kara Seas, via the advection by the North Atlantic Current (NAC). The role of the NAC on the sea-ice edge variability in the Atlantic sector was confirmed later by other observational studies (e.g. Furevik, 2001; Schauer *et al.*, 2002; Ingvaldsen *et al.*, 2004a, 2004b) and was also obtained in model studies (e.g. Goosse *et al.*, 2002; Winton, 2003; Zhang *et al.*, 2004; Goosse and Holland, 2005; Holland *et al.*, 2006; Jungclaus and Koenigk, 2010; Årthun *et al.*, 2012). Schlichtholz (2011), using observations covering the 1982–2006 period, estimated that about 75% of the winter SIE variability in the Nordic Seas is explained by the summer Atlantic water temperature in the

Barents Sea Opening (BSO, 13–17°E, 70–76°N). The significant link between the summer BSO temperature and the following winter SIE variability in the Greenland Sea suggests a role for westward advection by the Return Atlantic Current south of Spitsbergen.

Various modelling studies have shown an impact by the Atlantic thermohaline circulation on the SIT and SIE in the Labrador, Greenland, Barents and Kara Seas in multicentury present-day simulations (e.g. Holland *et al.*, 2001; Koenigk *et al.*, 2013). As the variability in the Atlantic meridional overturning circulation and subpolar gyre are themselves partially driven by sea-ice conditions in the Labrador and Nordic Seas (e.g. Mysak *et al.*, 1990; Wohlleben and Weaver, 1995; Yang and Neelin, 1997; Holland *et al.*, 2001; Escudier *et al.*, 2013), memory on decadal time-scales can arise from the ocean and sea-ice interactions. The ocean therefore appears as the main source of sea-ice predictability for time-scales beyond a few months in the Atlantic sector.

Although fewer studies have focused on the oceanic impact on the sea-ice edge in the Pacific sector, observational data indicated a crucial role of the warm water inflow through the Bering Strait, which accounted for about one-third of the sea-ice melt in 2007 (Woodgate *et al.*, 2010). The sea-ice cover in the Sea of Okhotsk and in the Bering and Chukchi Seas are particularly sensitive to the inflow of Pacific warm waters.

2.5. *Re-emergence*

Re-emergence of sea-ice anomalies can extend the sea-ice predictability limit. Each re-emergence mechanism described below for a given sea-ice variable relies mainly on the persistence of another variable. As a breakthrough, Blanchard-Wrigglesworth *et al.* (2011a) highlighted two different mechanisms for the re-emergence of SIA anomalies on time-scales from a few months up to 1 year: one mechanism explaining the re-emergence from the melt season to the growth season due to the persistence of sea-surface temperature (SST) anomalies; and the other one explaining the re-emergence from the growth season to the melt season because of the persistence of SIT anomalies. Their analyses are based on lagged correlations performed on the NSIDC sea-ice observations, the Hadley Centre Global Sea Ice and Sea Surface Temperature (HadISST) observations and a 30-member ensemble simulation performed with the CCSM3 climate model. Furthering the idea of the SIT persistence, Chevallier and Salas-Mélia (2012) highlighted a mechanism for the winter preconditioning of the summer sea-ice cover due to the survival of thick ice through the melt season. This mechanism has been determined from a 400-year-long pre-industrial control simulation run with the CNRM-CM3.3 climate model and it is the most promising mechanism in terms of variance explained for the pan-Arctic SIA up to 6 months in advance.

2.5.1. *Re-emergence from the melt season to the growth season: persistence of SST anomalies*

Evidence for this mechanism of re-emergence has been found by Blanchard-Wrigglesworth *et al.* (2011a) in both the CCSM3 climate model and observations. In the vicinity of the sea-ice edge, the SIA anomalies are associated with SST anomalies during the melt season. These SST anomalies persist during the summer after the sea ice retreats and they impact on the sea-ice cover when the sea-ice edge advances back to the same vicinity during the next autumn. A negative (positive) SIA anomaly in spring is associated with a positive (negative) SST anomaly along the sea-ice edge, which favours a negative (positive) SIA anomaly when the sea-ice cover returns during the next autumn. As a result, re-emergence is seen between pairs of months that share similar sea-ice coverage between the melt and the growth season: July–October, June–November, and May–December. Figure 6 illustrates this re-emergence mechanism in observational datasets and shows that this mechanism is present in observations until

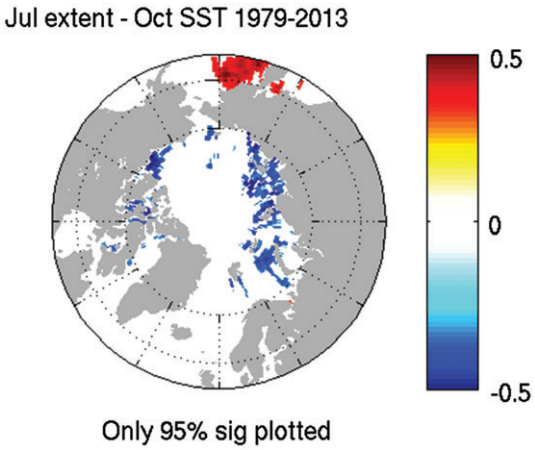

Figure 6. Correlation over the 1979–2013 period between the linearly detrended July total Arctic sea-ice extent (spatially integrated quantity) from NSIDC and the linearly detrended grid-point sea-surface temperature anomalies (spatially resolved quantity) in the following October from HadISST. Only the regions where the correlation is significant to the 95% level using a two-tailed Student's t test are shown.

October. Thereafter the SSTs are generally uncoupled from spring sea-ice anomalies. In the CCSM3 model, the SST anomalies associated with spring SIA anomalies are longer lived, which leads to a longer-lived re-emergence of SIA anomalies. This mechanism of re-emergence from the melt to the growth season was confirmed by Day *et al.* (2014) in four GCMs albeit with different magnitudes, and by Chevallier and Salas-Melia (2012), who estimated that 32% of the SIA variance, measured by the SLAC, could be explained by this mechanism in the CNRM-CM3.3 climate model (see their figure 5(a)). Similar results were also obtained by Schlichtholz (2011), from observations, along the sea-ice edge in the Norwegian and Barents Sea. According to Day *et al.* (2014), this re-emergence mechanism is also valid for the Arctic SIV.

2.5.2. *Re-emergence from the growth season to the melt season: persistence of ice thickness anomalies*

Evidence for this mechanism of re-emergence has been found by Blanchard-Wrigglesworth *et al.* (2011a) in the CCSM3 climate model. At present, observations of SIT are not available over a long enough period to verify this mechanism. During the growth season, local SIA anomalies are associated with local SIT anomalies in the vicinity of the sea-ice edge. Those SIT anomalies persist during the winter in the seasonal ice zone and they impact on the SIE locally, but also with a signature on the integrated Arctic SIE, when the sea-ice edge returns to the same vicinity during the next spring. A positive (negative) SIA anomaly in the growth season is associated with an early (late) date of freeze up, locally creating a positive (negative) SIT anomaly that slows down (accelerates) the sea-ice retreat during the next spring and is therefore associated with a local positive (negative) SIA anomaly. Re-emergence is therefore seen from January to April, from December to June, from November to July and from late summer (July–October) to the following September. Figure 7 illustrates such a re-emergence mechanism in CCSM3 for both cold season re-emergence (January to April) and summer-to-summer re-emergence (September to the following September). This mechanism of re-emergence from the growth season to the melt season was confirmed by Day *et al.* (2014) in four climate models, and by Chevallier and Salas-Mélia (2012) using the CNRM-CM3.3 climate model. Blanchard-Wrigglesworth *et al.* (2011b) complemented their first study by illustrating the contrast of a high simultaneous correlation between the pan-Arctic SIV and SIA during the summer season, with a low correlation the rest of the year in the CCSM4 climate model (Gent *et al.*, 2011). Chevallier and Salas-Mélia (2012) estimated, however, that the

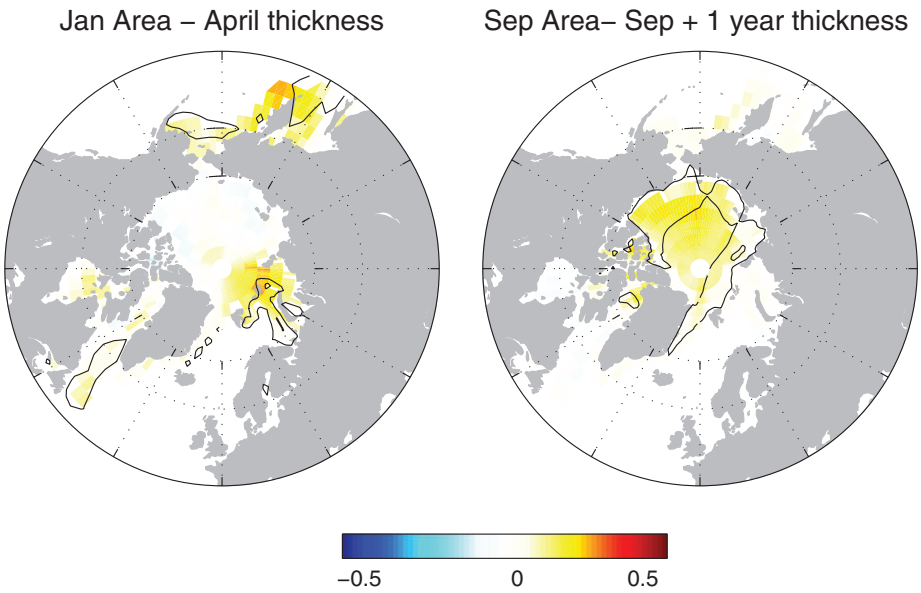

Figure 7. Correlation between (left) the linearly detrended January total Arctic sea-ice area (SIA; spatially integrated quantity) in CCSM3 and the linearly detrended sea-ice thickness (SIT) anomalies (spatially resolved quantity) in the following April in CCSM3 and (right) the detrended September SIA in CCSM3 and the detrended SIT anomalies in the following September (1 year lag) in CCSM3. Only the regions where the correlation is significant to the 95% level using a two-tailed Student's t test are shown. Contours show the areas where the SIC standard deviation exceeds 0.15 in (left) April and (right) September.

pan-Arctic SIV variance does not explain more than about 25% of the synchronous SIA variance, or more than 32% of the SIA variance 2–3 months in advance. The percentage of the SIA variance explained by the SIV variance decreases afterwards as the lag increases. The SIV is, however, a better predictor than the SIA for the July–November SIA 6–10 months in advance.

Blanchard-Wrigglesworth *et al.* (2011a) found that the summer-to-summer re-emergence of Arctic SIA anomalies weakens slightly under climate change, whereas Holland *et al.* (2011) found a substantial loss of predictability in SIA in future projections. Blanchard-Wrigglesworth *et al.* (2011a) also highlighted that seasonal re-emergence from autumn to spring and from spring to autumn appears to be unaffected by the sea-ice thinning.

2.5.3. Winter preconditioning for the summer season: memory in the ice-thickness distribution

Chevallier and Salas-Mélia (2012) showed in the CNRM-CM3.3 climate model that the area covered by relatively thick ice (thicker than 0.9–1.5 m) is a better predictor than the total SIA itself for the late spring until early autumn SIA a few months in advance. For example, the March area of ice thicker than 1.5 m explains 30% (40%) of the variance in the September (August) total SIA. The June area of ice thicker than 0.9 m (1.5 m) explains 76% (57%) of the variance in the September total SIA. Whereas the thinnest ice melts during spring and summer, thick ice persists until the end of the summer (Figure 8). This mechanism can be properly represented only in multicategory sea-ice models, i.e. models that diagnose an ice-thickness distribution (ITD, see appendix) over each grid cell instead of a single uniform thickness (Thorndike *et al.*, 1975; Bitz *et al.*, 2001; Lipscomb, 2001). Indeed, such models can transfer thick ice to the thin-ice categories during the melt season and make it persist, whereas that from thin-ice categories melts. Under a changing climate, the predictability brought by this winter preconditioning mechanism might decline due to the emptying of the thicker ice categories. This is consistent with the conclusions from Holland *et al.* (2008) and Goosse *et al.* (2009).

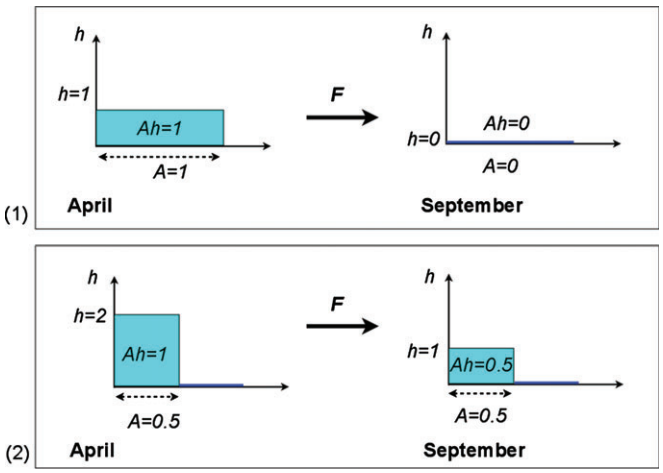

Figure 8. Schematic illustration of the preconditioning of the summer sea-ice area by the winter sea-ice thickness (SIT). Each panel represents the impact of an atmospheric forcing F on a grid cell of surface 1 m^2, covered by sea ice over an area A (m^2, x-axis) with thickness h (m, y-axis). The surface of open water is $1 - A$, and the initial grid-cell ice volume is $V = A \times h$ (m^3) $= 1$ m^3 in both panels. As in case 2 the initial SIT is $h = 2$ m, $h = 1$ m and $V = 0.5$ m^3 survive to the forcing F, which induces a vertical melting of 1 m, whereas no ice survives the forcing F in case 1, where the initial SIT is $h = 1$ m.

3. Predictability limit estimates

The previous section has suggested that knowledge of the Arctic climate conditions at some initial time could provide some information about the future state of the Arctic sea-ice conditions, through the memory/propagation of this initial information during the forecast. Potential predictability arising from the initial conditions can be estimated by initializing ensemble pseudo-predictions from a reference simulation after slightly perturbing the state selected from the reference simulation (Koenigk and Mikolajewicz, 2009; Holland *et al.*, 2011; Blanchard-Wrigglesworth *et al.*, 2011b). The distance between each realization of an ensemble pseudo-prediction and the reference simulation allows us to quantify to what extent the climate signals in the reference simulation would be potentially predictable with an operational forecast system, if the simulated processes matched perfectly the observed ones. A quantification of the potential predictability can be obtained through the potential prognostic predictability (PPP), which compares the ensemble spread with the internal variability in the reference simulation, or through the anomaly correlation coefficient (ACC), which correlates the anomalies from the different members and/or from the ensemble mean, or through the root mean square error

(RMSE), which measures the distance between the members and/or between the ensemble mean and the members. An extensive discussion of the various metrics available to estimate the potential skill is provided by Hawkins *et al.* (2014) in this same issue. This experimental design provides an upper bound for the prediction skill in a forecast system.

3.1. *Pan-Arctic integrated quantities*

3.1.1. *Sea-ice area and extent*

Using this experimental approach, the potential predictability of the monthly mean pan-Arctic SIA and SIE (Figure 9(a)), which exhibit similar predictability properties, has been estimated to be continuously significant for 1–2 years and intermittent up to 4 years ahead (Blanchard-Wrigglesworth *et al.*, 2011b; Day *et al.*, 2014; Tietsche *et al.*, 2014) in different coupled GCMs (CGCMs). Larger skill was obtained during the summer or winter seasons than during the transition seasons in terms of PPP or ACC (Holland *et al.*, 2001; Tietsche *et al.*, 2014), with even a re-emergence of skill in summer (Holland *et al.*, 2011) or winter (Day *et al.*, 2014) following the transition seasons. In terms of RMSE, the re-emergence of skill rather occurred at the onset of the freezing season when the amplitude of the variability decreases (Blanchard-Wrigglesworth *et al.*, 2011b; Tietsche *et al.*, 2014). It is worth highlighting the agreement between the various CGCMs in spite of their different mean states and variability (Tietsche *et al.*, 2014). The skill of dynamical predictions has been shown to be larger than the skill of persistence-based statistical predictions during the first 1–1.5 years (Day *et al.*, 2014). The potential predictability of the decadal mean Arctic SIE was also found to be significant (Koenigk *et al.*, 2012). Holland *et al.* (2011) estimated that the increase in spread between the ensemble members is mainly driven by thermodynamical processes (frazil, basal ice formation, snow-to-ice conversion, surface, basal and lateral melting), especially during summer.

3.1.2. *Sea-ice volume*

The potential predictability of the monthly mean pan-Arctic SIV (Figure 9(b)) has been shown to be continuously significant for at least 4 years (Blanchard-Wrigglesworth *et al.*, 2011b; Day *et al.*, 2014; Tietsche *et al.*, 2014). Greater skill was obtained in winter than in any other season in terms of PPP, ACC or RMSE (Holland *et al.*, 2011; Blanchard-Wrigglesworth *et al.*, 2011b; Day *et al.*, 2014). This feature could be explained by the negative ice-thickness growth-rate feedback (Bitz and Roe, 2004), which limits the error growth during winter. A larger ACC skill in SIV was obtained for those CGCMs exhibiting the largest fraction of variability on decadal time-scales (Tietsche *et al.*, 2014). The skill of dynamical predictions has been shown to be larger than the skill of persistence-based statistical predictions during the first few months only (Day *et al.*, 2014). The potential predictability of decadal mean Arctic SIV was, however, found not to be significant (Koenigk *et al.*, 2012), but this estimate was based on one model only.

3.2. *Spatial distribution*

The potential predictability limits of integrated quantities such as the Arctic SIA, SIE and SIV mask out regional disparities in the duration of potential predictability. The existing studies on this topic have analysed monthly, seasonal, annual and decadal mean fields. In this section, studies are separated by this criterion because changing the averaging time-scale changes the signal-to-noise ratio, therefore potentially affecting the results.

3.2.1. *Monthly means*

In a set of ensemble pseudo-predictions, initialized in July, with four different CGCMs, the smallest September SIC and SIT prediction errors were consistently found in the central Arctic, whereas the largest prediction errors were found in the MIZ (Tietsche *et al.*, 2014). During the following March, the SIC prediction errors were largest along the climatological ice edge in the Atlantic and Pacific Oceans and small in the Arctic Ocean, while the SIT prediction errors were largest along the coastlines of the Arctic Ocean and smallest in the interior Arctic and in the marginal seas. The amplitude of the SIT errors differed substantially between the CGCMs. The growth of SIT prediction errors was dominated by advective processes mainly due to wind errors (Tietsche *et al.*, 2014). Advective processes explained the discrepancy between the CGCMs: the larger the climatological ice thickness, the larger the error associated with the advective tendency. A drop in predictive skill occurred in the second prediction year. In one of these models, Day *et al.* (2014) found significant SIE predictive skill for 1–2 years in the MIZ. The time-scale of potential predictability was longer on the Atlantic side than on the Pacific side, with the longest duration of significant skill in the Labrador Sea. The SIE predictive skill was significant only during the first summer in the seas of the Arctic Ocean with perennial sea-ice cover.

3.2.2. *Seasonal means*

In the central Arctic, Laptev and East Siberian Seas, the seasonal mean SIT was found to be highly predictable due to persistence,

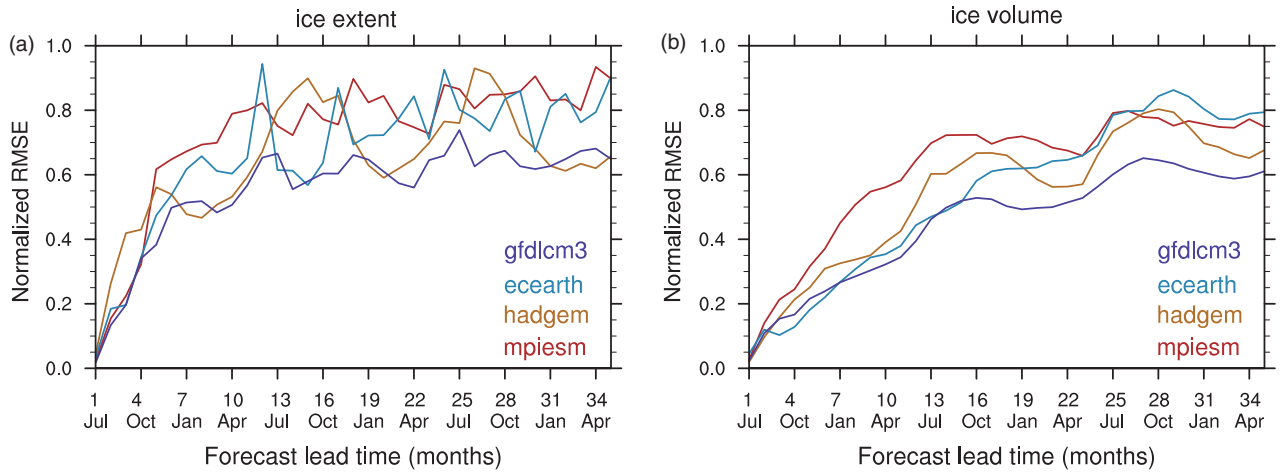

Figure 9. Normalised root mean square error (RMSE) for predictions of (a) Arctic sea-ice area and (b) Arctic sea-ice volume for four different CMIP5-class atmosphere–ocean general circulation models. Normalization is carried out by dividing the RMSE by $\sqrt{2}\sigma$, where σ is the standard deviation of the linearly detrended control run in the corresponding month. The normalized RMSE is 1 when there is no skill in the predictions.

whereas the SIC exhibits very low predictability (Koenigk and Mikolajewicz, 2009). Another modelling study, Germe *et al.* (2014), found strong contrast in predictability between the Atlantic and Pacific sectors: in the GIN (Greenland, Iceland, Norwegian) and Labrador Seas, the winter SIE is potentially predictable up to 10 years, whereas in the Okhotsk, Barents and Bering Seas, it is only predictable during the first forecast year. A similar contrast was obtained for SIV (Germe *et al.*, 2014). In a different model, the PPP was found to be significant up to 1 year ahead for seasonal mean SIC and SIT in the Barents, Kara, Greenland and Iceland Seas and 2 years in the Labrador Sea, the predictability being dominated by dynamic processes in the later region (Koenigk and Mikolajewicz, 2009).

3.2.3. *Annual means*

Koenigk and Mikolajewicz (2009) showed that the annual mean SIT is highly predictable in the Central Arctic for at least 2 years ahead, mainly due to persistence, while the SIC predictability is very low there. In the Barents, Kara, Greenland and Iceland Seas, both annual mean SIT and SIC were found significantly predictable the first year (Koenigk and Mikolajewicz, 2009). Furthermore, Koenigk and Mikolajewicz (2009) showed that the annual SIT predictability exceeds predictability arising from persistence along the Transpolar Drift Stream, the East Greenland Current and the Labrador Sea during the first 2 years in agreement with the advection characteristics described in section 2.2. The annual mean sea-ice export through Fram Strait was found significantly predictable up to 2 years ahead (Koenigk and Mikolajewicz, 2009).

3.2.4. *Decadal means*

Koenigk *et al.* (2012) found a potential predictability of decadal mean SIT and decadal mean SIC confined to the Labrador, Greenland, Barents and Kara Seas. This skill seemed to be related to the AMOC in agreement with the results discussed in section 2.4.

3.3. *Dependence of the skill on the month of initialization*

3.3.1. *Pan-Arctic integrated quantities*

Blanchard-Wrigglesworth *et al.* (2011b) found similar levels of predictability of the monthly mean pan-Arctic SIE and SIV when initializing in September or January for the following spring and beyond, suggesting that predictions of the summer sea-ice cover could be made as early as the autumn. Day *et al.* (2014) found that the prediction skill of pan-Arctic SIE and SIV declined more rapidly during the first 4 months when the predictions were initialized in May, compared with those initialized in January or July. This melt-season 'predictability barrier' followed by a re-emergence of skill during the next 5 months is consistent with section 2.1. Predictions of the Arctic summer SIV and SIE were, however, more skilful when initialized from the previous May rather than the previous January (Day *et al.* 2014).

3.3.2. *Regional quantities*

Day *et al.* (2014) found that summer monthly mean SIE in the Kara, Laptev and East Siberian seas was predictable only from simulations initialized in July (not from January or May). Koenigk and Mikolajewicz (2009) also obtained a higher predictability of the annual mean SIC along the Arctic coasts when initialized in July rather than January, mainly thanks to persistence. In the GIN, Barents and Labrador Seas, the skill in predicting the monthly mean SIE (Day *et al.*, 2014) when initialized in May and July was indistinguishable after 3–4 months and it was significant for longer when initializing in January rather than in May or July. Koenigk and Mikolajewicz (2009) also found that, in the Labrador Sea, Hudson Bay and Bering Sea, the predictability of both the annual mean SIT and SIC was much higher during the first year when initialized in January rather than in July. As no sea ice is present in those regions in winter, sea-ice predictability depends greatly on the formation in the following winter when initialized in July. Beyond the first prediction year, the predictive skill for annual means was not sensitive to the initialization month.

3.4. *Impact of climate change on sea-ice predictability*

Since the 1970s, pan-Arctic SIE has been shrinking in all months and this is expected to continue into the future (Serreze *et al.*, 2007; Stroeve *et al.*, 2012). Changes in climate can modify the variability and predictability properties of the sea ice. Comparing three case studies, Holland *et al.* (2011) estimated that the thicker the initial sea-ice cover, the higher the subsequent monthly SIA potential predictability, which is consistent with the role of SIT on SIA predictability highlighted in section 2.5. Germe *et al.* (2014) also found that the potential winter SIE predictability in the GIN Seas decreased during the past 50 years or so, mostly due to the narrowing of the Greenland MIZ (Strong, 2012). However, Holland *et al.* (2011) found higher monthly SIV potential predictability for thinner sea-ice initial conditions (in contrast to the monthly SIA). The lower efficiency of the negative ice-thickness growth-rate feedback for a thick sea-ice cover (Bitz and Roe, 2004) could explain a larger error growth rate for thick ice cover. Germe *et al.* (2014), however, obtained a decreased SIT predictability in the central Arctic with reduced sea-ice cover, with a larger set of start dates and a different model.

3.5. *Predictability arising from the external radiative forcings*

The climate change caused by changes to external radiative forcings does not only modify the predictability properties of sea ice, but also provides a source of potential predictability in addition to that arising from the memory of the initial conditions. Using six transient reference simulations rather than a stable reference simulation, Blanchard-Wrigglesworth *et al.* (2011b) assessed the contributions of both sources of predictability. For SIV, the externally forced predictability has been estimated to increase with forecast time and exceeds the potential predictability arising from the initial conditions from year 4 onward. For SIA, potential predictability from the external radiative forcing appeared only from year 5, leaving a gap in potential predictability between years 2 and 5 (Blanchard-Wrigglesworth *et al.* 2011b).

3.6. *Predictability of extreme anomalies*

Some CGCMs simulate rapid ice-loss events in their twenty-first century projections, and such events are of huge societal importance. Holland *et al.* (2011) investigated the predictability of a drastic reduction in September Arctic SIA by 1.45 million km^2 in CCSM3. This substantial sea-ice loss was captured (although not its amplitude) by every single member of a pseudo-prediction ensemble initialized on the preceding 1 January as a result of the preconditioning of anomalously thin ice in the Beaufort, Chukchi and East Siberian seas.

Tietsche *et al.* (2013a) investigated the predictability of two extreme negative sea-ice anomalies in a climate-change projection in MPI-ESM produced under a moderate-emission scenario. Although the onset of the extreme anomalies was not predictable, predictions initialized after the onset captured the strengthening of the anomalies until 1 year ahead. Tietsche *et al.* (2013a) additionally assessed to what extent simple initialization methods exploiting the current observational network could allow realizing the potential predictability level by performing two sister ensembles: one control ensemble using slightly perturbed initial conditions and one sensitivity ensemble using initial conditions obtained by assimilating sea-ice data (Tietsche *et al.*, 2013b) from the reference simulation into another realization

of a climate-change projection under the same scenario. The performance when assimilating sea-ice data is close to that obtained when using perturbed initial conditions.

4. Predictions on seasonal to decadal time-scales

4.1. *Initialisation issues*

The studies presented in the previous section estimated the level of sea-ice predictability under the assumptions of a perfect knowledge of the initial conditions and/or a perfect representation of the processes leading to predictability in climate models. The violation of these assumptions raises a number of issues discussed in this section.

4.1.1. *Sparse observational coverage and sea-ice data assimilation*

Up to 1973, the Arctic sea-ice data are limited to monthly estimates of SIE, with complete cover assumed within the ice pack and a necessary treatment of missing data in the marginal seas (Walsh and Johnson, 1979). From 1973, the US Navy, Canadian and Danish aerial reconnaissance provided quasi-weekly estimates of SIC (Knight, 1984). The advent of satellite microwave imagery in 1978 allowed for retrieving SIC at a 2 day frequency, increased to a daily frequency in 1987, and roughly at a 1° resolution (Cavalieri *et al.*, 1996). The publicly distributed SIC datasets, the National Snow and Ice Data Center (NSIDC) (Cavalieri *et al.*, 1996; Fetterer *et al.*, 2002) one covering the 1978–present period and the HadISST (Rayner *et al.*, 2003) one covering the 1870–present period, stand as the best estimates obtained from combination, homogenization and extrapolation of these sparse observational data. The SIT data are much scarcer (Kwok and Rothrock, 2009): the first unified dataset (Lindsay, 2010) was released in 2010. It combines Arctic observations by submarines from 1975, moored upward-looking sonar from 1990 and airborne or satellite electromagnetic measurements in the past decade. A complete and coherent description of the sea-ice state can be obtained only through a physical extrapolation of the sparse observations, relying on the equations that describe the sea-ice dynamics and thermodynamics.

The first attempt at providing such a complete description of the sea-ice state was performed by Lisaeter *et al.* (2003) by assimilating SIC data in a coupled ice–ocean model every week over more than 1 year using an ensemble Kalman filter (Evensen, 1994). Their assimilation procedure led to the largest updates of the ocean and sea-ice variables along the sea-ice edge, and to larger updates in the central Arctic in summer than in winter.

Sea-ice velocity is well observed in the recent decades, and its assimilation can be used to improve the simulated SIT, as shown by Zhang *et al.* (2003) by applying an optimal interpolation procedure to assimilate buoy motion and satellite ice-motion data in an ice–ocean model. Lindsay and Zhang (2006) combined the velocity assimilation scheme by Zhang *et al.* (2003) with a nonlinear nudging scheme for SIC that substantially corrects the SIC when large differences between the model and the observational data are seen, i.e., along the sea-ice edges. The three-dimensional variational assimilation technique was tested by Caya *et al.* (2010) on a regional ice–ocean model. They showed significant improvements over a simple nudging technique when combining multiple sources of observational data.

The propagation of the analysis update from the observed fields to the unobserved fields, such as the SIT, remains an issue. Dulière and Fichefet (2007) assessed the performance of an optimal interpolation procedure to simultaneously assimilate SIC and velocity. They obtained an optimal propagation of the SIC analysis information to the SIT field when conserving (not conserving) the ice volume in a grid cell in the case of dynamically (thermodynamically) caused model errors. Tietsche *et al.* (2013b) concluded that the best performance in propagating the SIC analysis information to the SIT field is obtained when using a fixed proportionality coefficient between the mean thickness and the concentration analysis updates, rather then when using analysis updates with conserved mean thickness or with conserved actual thickness. The combined obstacles of the bounded nature of the SIC and of the need for coherence between SIC and SIT analyses, whereas SIT data are much sparser than SIC data, make the sea-ice assimilation a highly challenging task.

To date, the most widely distributed coupled ice–ocean reanalysis and the most widely used as a reference, is the PIOMAS (Pan-Arctic Ice Ocean Modelling and Assimilation System; Schweiger *et al.*, 2011) reanalysis in which the SIC from the ERA40 and operational analyses is assimilated via the nonlinear nudging scheme from Lindsay and Zhang (2006). The SST from the ERA40 and operational analyses is also assimilated via a nudging scheme with a 15 day relaxation time. The reanalysis covers the Arctic, North Atlantic and North Pacific with a resolution of 22 km.

4.1.2. *Overcoming the initial shocks and drift*

When running predictions, using initial conditions from reanalysis products produced with a different model, or using inconsistent sources of initial conditions for the various components (atmosphere, ocean, sea ice) of the climate system can lead to initial shocks in the prediction. For this reason, the various institutes developing sea-ice prediction systems put efforts into designing sea-ice reconstructions with the available observational datasets and reanalysis suitable for their forecast system.

For example, the sea-ice predictions produced with the CNRM-CM5.1 (Chevallier *et al.*, 2013) and the EC-Earth 2.3 (Guemas *et al.*, 2014) global coupled climate models were initialized from sea-ice reconstructions produced with their respective sea-ice components. The ocean and sea-ice coupled models were forced with the surface atmospheric fields from the European Centre for Medium-range Weather Forecasts (ECMWF) reanalyses used to initialize the atmospheric component in the sea-ice predictions afterwards. Whereas Chevallier *et al.* (2013) used the ocean state from the sea-ice reconstructions to initialize the oceanic component, Guemas *et al.* (2014) additionally nudged the ocean temperature and salinity during the sea-ice reconstruction toward their counterpart from the NEMOVAR-ORAS4 reanalysis (Mogensen *et al.*, 2011; Balmaseda *et al.*, 2012b), and they used the NEMOVAR-ORAS4 reanalysis to initialize the oceanic component afterwards. With both approaches, the sea-ice initial state for the prediction is constrained only by atmospheric and/or oceanic observational data, and not by sea-ice data. Both approaches also ensure a relative consistency between the initial oceanic, atmospheric and sea-ice states. It is not a perfect consistency though because the atmospheric and oceanic reanalyses were not provided with any information about the sea-ice reconstructions at production time.

The sea-ice predictions produced with the National Center for Environmental Prediction (NCEP) Climate Forecast System version 2 (CFSv2; Saha *et al.*, 2010) and with the Canadian Seasonal to Interannual Prediction System (CanSIPS; Merryfield *et al.*, 2013a) are initialized from weakly coupled atmosphere–ice–ocean climate reanalyses produced with the same climate model as that used to generate the predictions. To initialize the sea-ice component of the CFSv2 system, observed SICs from satellite only are assimilated. The response of the sea-ice model to atmospheric and oceanic forcing determines the SIT. To initialize the CanSIPS system, the SIC is nudged toward the interpolated monthly HadISST dataset and the SIT is relaxed to the model climatology.

When focusing on decadal time-scales, the emphasis has been put, up to date, on the initialization of the oceanic component, which holds most of the memory. Germe *et al.* (2014), for example, obtained the initial climate state from a historical

simulation performed with the same coupled model as used in the predictions but in which the ocean temperature and salinity was restored toward their counterpart from the NEMOVAR-COMBINE reanalysis (Balmaseda *et al.* 2012a).

Finally, even if initialized from consistent atmospheric, oceanic and sea-ice state, typical dynamical sea-ice predictions are affected by a strong drift of the model, which develops its biases. Such systematic error can be corrected a posteriori by assuming a linear superposition of the drift and the climate signal to be predicted. Initializing from observed anomalies added to model climatology instead of initializing from observations, i.e. the so-called anomaly initialization approach, has been suggested to greatly reduce the drift and therefore its interaction with the climate signal to be predicted. This initialization technique assumes though an independence of variability on the mean state. Such an approach has not been tested on sea-ice predictions yet and raises a number of challenges due to the bounded nature of sea-ice variables and to the need for an accurate estimation of the model and observed climatologies. Alternative anomaly initialization techniques need to be developed and tested for sea-ice predictions, for example by translating the observed anomalies from the observed sea-ice edge to the model sea-ice edge.

4.1.3. Ensemble generation methods

Chevallier *et al.* (2013) and Germe *et al.* (2014) produced respectively nine- and ten-member ensembles by initializing with different atmospheric conditions from the initial month of the prediction, but with identical ocean and sea-ice conditions for all members. Du *et al.* (2012), however, found a larger ensemble spread in the Arctic SIA when introducing perturbations in the ocean initial conditions, the spread therefore being more representative of the forecast error. Using a similar lag-based approach to Chevallier *et al.* (2013) and Germe *et al.* (2014), Wang *et al.* (2013) produced 16-member ensembles that were initialized using 16 different initial conditions taken from successive dates prior to the initial date of a prediction from the full climate state of the CFSR reanalysis. Sigmond *et al.* (2013) attempted, for the first time, to sample the uncertainty in the sea-ice initial conditions by generating a 20-member reanalysis in which each member was nudged toward the exact same atmospheric, oceanic and sea-ice analysis. Guemas *et al.* (2014) further refined their methodology on capturing the uncertainty in the sea-ice state by introducing surface-wind perturbations to generate five different members in their sea-ice reconstructions and by nudging each member toward a different member of the NEMOVAR-ORAS4 reanalysis. Such a methodology produced a larger prediction ensemble spread in the sea-ice state of about 5–30%, which is more representative of the forecast error (Guemas *et al.* 2014).

4.2. Forecast skill on seasonal to interannual time-scales

4.2.1. Statistical forecasts

The first attempts to forecast Arctic sea-ice cover on seasonal time-scales relied on statistical forecast models constructed from the relationships in the historical record between atmospheric (Barnett, 1980; Walsh, 1980), oceanic (Johnson *et al.*, 1985) or sea ice (Walsh, 1980; Johnson *et al.*, 1985) predictors and the sea-ice variables to be predicted. End of summer ice conditions in the Beaufort Sea would be predictable from the spring total and winter multiyear SICs, the October East Atlantic Index and the March North Atlantic Oscillation phases, which jointly explain 85% of the sea-ice cover variance over the 1979–1999 period (Drobot and Maslanik, 2002). The pan-Arctic minimum SIE would be predictable as early as in February from the monthly SIC, surface skin temperature, surface albedo and downwelling long-wave radiation, which jointly explain 46% of its variance over the 1982–2004 period (Drobot *et al.*, 2006), although most of the skill originates from the SIC predictor. Drobot (2007) focused on predictions of the minimum SIE in the Beaufort–Chukchi Seas, the Laptev–East Siberian Seas, the Kara–Barents Seas, and the Canadian Arctic Archipelago (CAA) from the same predictors as Drobot *et al.* (2006) and obtained the lowest (highest) percentage of variance explained in the CAA (Beaufort–Chukchi Seas) of 44% (80%). Tivy *et al.* (2007) tested more than 1500 potential predictors for the summer sea-ice cover along the shipping routes of the Hudson Bay and obtained a 77% success rate in predicting the opening date over the 1972–2002 period based on the winter North Atlantic SSTs and 500 hPa geopotential heights.

Lindsay *et al.* (2008) built empirical statistical models for the pan-Arctic SIE based on multiple linear regressions of a wide range of predictors: observed atmospheric circulation indices, observed SIE and SIC together with the ocean temperature at various levels, the mean SIT and its distribution taken from the PIOMAS reanalysis. Their statistical models exhibited a greater skill in predicting the September SIE than those by Drobot *et al.* (2006) based on satellite observations only. The North Atlantic Oscillation, the Arctic Oscillation, the Pacific Decadal Oscillation and the Pacific North American index were found to have little value as predictors of the September Arctic SIE compared with ocean and ice predictors. Although the atmospheric circulation partly drives the simultaneous sea-ice cover variability, it has an impact on the longer lead times mainly through the memory of the ocean and sea ice. The SIC from July and August was established as the best predictor for the September Arctic SIE, whereas the area of thin ice and the mean SIT proved better predictors than the SIC from the previous spring and winter, which is consistent with the mechanisms described in section 2.5. The ocean variables were found to be the best predictors on lead times longer than 3 months, especially the autumn temperature at depths down to 300 m, mainly because they predicted the long-term trend. The trend in September SIE accounted for 76% of its variance and therefore provided most of the predictive information. Detrending the September SIE and all the predictors, no significant skill was found at more than a 3 month lead time (Lindsay *et al.*, 2008). For regional predictions from June to September, the greatest skill was found in the Barents, Kara and Greenland Seas. Lindsay *et al.* (2008), however, noted the limitation due to the non-stationarity of the relationships between the predictors and the predictands, illustrated also by Holland and Stroeve (2011) and Holland *et al.* (2001), which can be overcome only by using dynamical forecast systems.

4.2.2. Dynamical forecasts

The first ensemble dynamical prediction was performed by Zhang *et al.* (2008) based on the PIOMAS coupled ice–ocean model driven by the NCEP/NCAR (National Center for Atmospheric Research) forcing fields. Targeting the September sea-ice cover, they produced seven-member ensembles by forcing the PIOMAS model with the October–September historical atmospheric fields from the seven previous years. The ocean and sea-ice initial conditions were taken from a PIOMAS simulation in which observed SICs had been assimilated until the start date of the prediction. In the 2008 case, immediately following the last record low SIE at the time of publication, they illustrated the systematic (for each member) reduction in SIT over the Arctic region. This reduction reaches 1.2 m in the Canada Basin and Archipelago which was attributed to the initialization of the sea ice and ocean with observational data.

Wang *et al.* (2013) and Sigmond *et al.* (2013) improved the forecasting protocol by using CFSv2 and CanSIPS respectively, two atmosphere–ocean–sea-ice coupled climate systems, instead of using ocean and sea-ice components only (see sections 4.1.2 and 4.1.3 for the initialization). They performed a retrospective prediction exercise by initializing, over a period of at least 27 years, predictions every month of at least 10 months into the future.

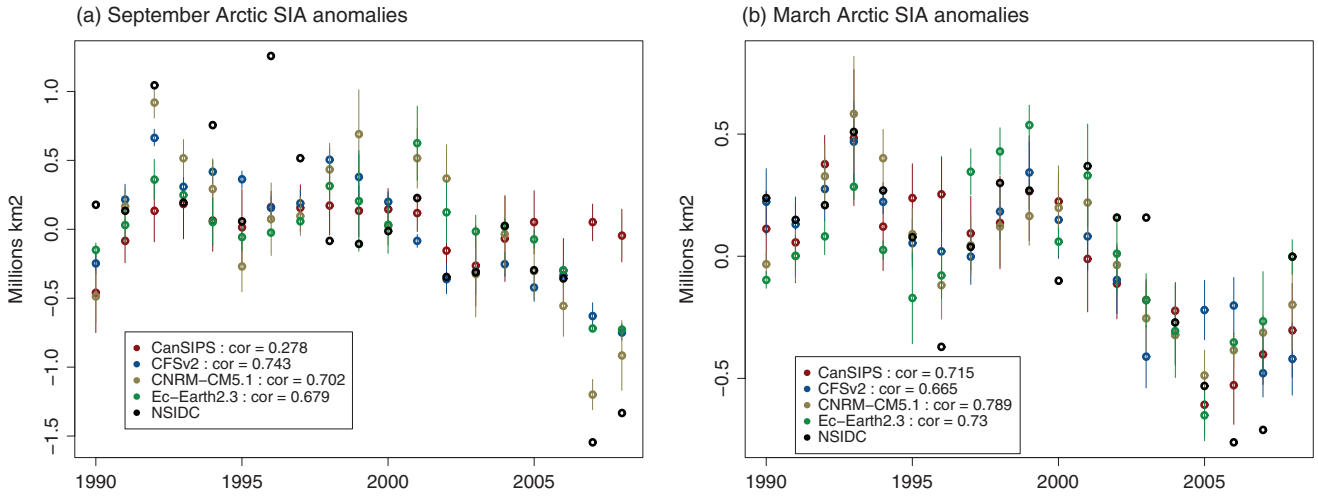

Figure 10. (a) September and (b) March Arctic sea-ice-area anomalies from the predictions initialized on (a) 1 May and (b) 1 November performed with the CanSIPS (red), CFSv2 (blue), CNRM-CM5.1 (yellow) and EC-Earth 2.3 (green) forecast systems and from the NSIDC observations (black). The dots indicate the ensemble means whereas the vertical bars indicate the interquartile range between the ensemble members. The correlation between the predicted and observed SIA is provided for each forecast system in the legend.

Both forecast systems generally outperformed a persistence-based statistical model. The CanSIPS forecast system had a generally lower skill than CFSv2 (Merryfield *et al.*, 2013b), which could be explained by the underestimated trend in HadISST used for initializing SIC, the use of a SIT climatology for initialization, and the absence of SIT categories in the sea-ice model. The RMSE of Arctic SIE was lower during the extended winter (November–May) season than during the summer (June–October) season in CFSv2, but the amplitude of the anomalies to be predicted are larger in summer. Up to lead times of 2 months, the ACC was higher during summer (June–October) than during the extended winter season (November to March) with both forecast systems. Sigmond *et al.* (2013) attributed the greater skill in summer to the larger trend for these months. The longer the lead time, the larger was the contribution to skill from the trend in CanSIPS. For lead times longer than 3 months, however, the ACC was higher in winter and spring (December–March) than in summer and early autumn (June–October) with CFSv2. In the detrended forecasts, the greatest skill was obtained in spring and summer up to a 3 month lead time for both CFSv2 and CanSIPS. Beyond and until a 1-year-lead time, the winter was the most predictable season and the only one with significant skill for both forecast systems. Modest skill was found in spring and autumn, synchronous with low persistence during these seasons (see section 2.1). The performances of CFSv2 and CanSIPS in predicting the September (March) SIA when initialized on 1 May (November) are illustrated in blue and red respectively on Figure 10.

Chevallier *et al.* (2013) performed 5-month-long predictions with the CNRM-CM5.1 global coupled climate model initialized on 1 May and 1 November each year during the 1990–2008 period. This dynamical forecast system captured the September and March SIE 5 months in advance, with correlations of 0.72 and 0.74 respectively, which fell to 0.60 and 0.53 after a linear detrending but were still significant to the 95% level. The CNRM-CM5.1 forecast system outperformed statistical forecasts based on the persistence of the SIE or the SIV, as well as the CanSIPS forecast system (Figure 10), although sea-ice observations were assimilated into the initial conditions of the latter. It shared similar performance with the CFSv2 forecast system. After detrending, whereas the greatest skill was found in winter at lead times beyond a few months with the CFSv2 and CanSIPS forecast systems, in CNRM-CM5.1 the greatest skill was found in summer. 50% of the variance of the September SIE in the seasonal forecasts from Chevallier *et al.* (2013) was explained by the area covered by thick ice (>1.5 m) in May, which is consistent with the mechanism of winter preconditioning described in section 2.5. 22% of the variance of the March SIE was explained by the October North Pacific SST (30°N–70°N). This dynamical forecast system captured the 2007 September SIE as the record minimum over the re-forecasted period (yellow in Figure 10), including the ice bridge between the central Arctic and northern Siberia, albeit with slightly too much ice toward the Chukchi and East Siberian Seas.

Combining the predictions from multiple forecast systems has been shown to generally increase the forecast skill compared with the skill of each single forecast system (Hagedorn *et al.*, 2005). Merryfield *et al.* (2013b) applied this concept for the first time to Arctic SIA by combining the CFSv2 and CanSIPS predictions initialized every calendar month from 1982 to 2009, and showed that the combination of those two forecast systems outperformed both considered individually, in terms of ACC and RMSE. Most of the skill originated from the long-term trend. A significant ACC skill in detrended anomalies was found for the first 2–3 months, except in late autumn and winter when the skill was significant up to 10 months lead time. The largest added value of the combined forecast systems relative to a persistence model was found for the prediction of winter months up to a 7 month lead time and in the prediction of summer conditions (June–September) from a spring (April–May) initialization.

4.3. *Forecast skill on interannual to decadal time-scales*

Guemas *et al.* (2014) assessed the skill in seasonal-mean sea-ice cover up to 3 years lead time in the EC-Earth 2.3 forecast system using 28 3-year-long predictions initialized on 1 November of different years from 1960 to 2010 (green in Figure 10). Their refined methodology compared with that used by Chevallier *et al.* (2013) to generate an ensemble of sea ice reconstructions (see section 4.1.2) allowed for a reduced RMSE in Arctic SIA by about 5–10% and in near-surface temperature by up to 50% locally, as assessed through a sensitivity experiment to the initialization methodology. The pan-Arctic SIA signal superimposed on the long-term trend could be predicted with a significant ACC until a 6 month lead time with a re-emergence of skill at a 1 year lead time. Germe *et al.* (2014) assessed the skill in predicting the winter mean sea-ice cover in the various Arctic Seas in decadal climate predictions performed with the CNRM-CM5.1 forecast system. Significant skill in total Arctic SIV and SIE in summer and winter was obtained up to 10 years ahead, which corresponds to the length of the forecasts, but this skill mostly originated from the external forcings. Although not significant after a linear detrending, the initialization brought added skill for the first two forecast years when predicting the GIN and Labrador winter SIE and SIV, relative to the skill of a simple persistence prediction.

4.4. *The gap between potential and actual forecast skill*

Although the potential skill in predicting monthly mean pan-Arctic SIA and SIE that arises from the knowledge of the initial conditions has been estimated to be continuously significant for 1–2 years and intermittent up to 4 years (section 3.1.1), the actual skill of dynamical forecast systems is significant for only 3–5 months into the future when detrended (section 4.2), except for the winter season when it is significant up to 1 year ahead. The state-of-the-art dynamical forecast systems, however, tend to reach the level of potential skill arising from the external radiative forcings (section 4.3).

On regional scales, whereas the winter mean SIE is potentially predictable up to 10 years in the GIN and Labrador Seas (section 3.2), the actual forecast skill with the same model is significant only for the first 2 years at most (Germe *et al.* 2014).

5. Perspectives

Arctic sea-ice predictability mechanisms have been extracted from the short observational record combined with model studies. Disentangling the role of the various sources of predictability or how these roles evolve with climate change present a challenge given the sparse observational data available. Model studies can partially compensate for the lack of observations thanks to their ability to extrapolate the climate system behaviour under new conditions. Such an extrapolation, however, assumes a realistic behaviour that can be simulated only if enough observations are available for a thorough evaluation of the sea-ice processes in those models. Some inconsistencies still appear between climate models, for example in their estimates of the sensitivity of the total Arctic SIV predictability to changing Arctic conditions. The intensive observational campaign planned during the Year of Polar Prediction (YOPP) in 2017–2018 will stand as a crucial opportunity to validate further the state-of-the-art sea-ice models and improve their realism, which will contribute to a better understanding of the predictability mechanisms. The YOPP will also contribute to reducing the uncertainties in the atmospheric reanalyses over the Arctic Ocean that are used to generate sea-ice reconstructions. Hopefully, these efforts will result in an increase in prediction skill.

Predicting the Arctic sea-ice state requires the prescription of accurate sea-ice initial conditions. Further development and testing of assimilation methods that account for the bounded nature of the sea-ice fields and that propagate efficiently the information from the SIC to the SIT are still required. Observing system experiments (OSEs), which assess the impact of including or excluding a certain set of observations on forecast skill, have been conducted by the numerical weather-prediction community to optimize the atmospheric observational network (e.g. Cardinali, 2009). A co-ordinated set of similar experiments using a model simulation of pseudo-observations would be very informative on the optimal type and distribution of the observations required, as part of a long-term observation strategy, to improve sea-ice prediction skill. The ensemble techniques already tested to generate sea-ice reconstructions also need further refinement to account properly for the uncertainty in the sea-ice initial conditions, for example by introducing additional perturbations in the atmosphere or by subsampling the sea-ice observational data.

Finally, as an essential step toward operational sea-ice forecasting, the protocol to assess the predictive capabilities of state-of-the-art sea-ice forecast systems should be further developed: an increase in the ensemble sizes and in the number of start dates, an increase in the number of case studies, a multimodel comparison with the exact same experimental set-up and a systematic assessment of the performance in capturing the spatial patterns of SIT and SIC should all be considered. Such a spatial assessment of the performance would also allow for fostering the understanding of the predictability processes and of the model weaknesses.

Acknowledgements

The authors wish to thank Woo-Sung Lee and William Merryfield for sharing the sea-ice forecasts from the CanSIPS and CFSv2 forecast systems. This work was supported by the EU funded SPECS (FP7-ENV-2012-308378), the MINECO funded PICA-ICE (CGL2012-31987) projects and the Catalan Government.

Appendix

The Community Climate System version 2 (CCSM2; Kiehl and Gent, 2004) includes the dynamic–thermodynamic CICE sea ice model (Briegleb *et al.*, 2004; Hunke and Lipscomb, 2004), which uses an elastic–viscous–plastic rheology (Hunke and Dukowicz, 1997), resolves a subgrid-scale SIT distribution (Thorndike *et al.*, 1975; Bitz *et al.*, 2001; Lipscomb, 2001), and relies on the thermodynamics of Bitz and Lipscomb (1999). The ice-thickness distribution (ITD) is a probability density function $g(h)$ that describes the probability that the ice cover over a given region has thickness h. The processes controlling the ITD are ice growth, melt, divergence, ridging and advection. The ice thickness space is discretized into N ice-thickness categories. For each time step, N equations are solved, and the ice transfers from one category to another are handled in a way conserving volume, area and energy. Bitz *et al.* (2001) showed that between five and ten sea-ice categories are needed to capture the effect of an ITD on SIV. The CCSM3 climate model (Collins *et al.*, 2006) is an upgraded version of CCSM2. Both models have a resolution of about 1° for the seaice model in the Arctic Ocean.

The PIOMAS (Schweiger *et al.*, 2011) coupled ice–ocean reanalysis is based on the Parallel Ocean and Ice Model (Zhang and Rothrock, 2003). The multicategory ice thickness and enthalpy distribution (TED) sea-ice model (Zhang and Rothrock, 2001) consists of five main components:

- a momentum equation that determines the ice motion
- a viscous–plastic ice rheology that determines the internal ice stress
- a heat equation that determines ice temperature profile and ice growth or decay
- an ice-thickness distribution equation that conserves the ice mass
- an enthalpy distribution equation that conserves ice thermal energy

The ECHAM5/MPI-OM coupled general circulation model (Marsland *et al.*, 2003; Roeckner *et al.*, 2003) includes a Hibler-type dynamic–thermodynamic sea-ice model with viscous–plastic rheology (Hibler, 1979). Its ocean resolution reaches a few tens of kilometres in the Arctic Ocean. The Max-Planck Institute Earth System Model Low Resolution coupled climate model (Mauritsen *et al.*, 2012) has a resolution of about 1.5° in the Arctic Ocean for its sea-ice component.

The CNRM-CM3.3 climate model (Salas-Mélia *et al.*, 2005) includes the Global Experimental Leads and Ice for Atmosphere and Ocean sea-ice model version 4 (GELATO4; Salas-Mélia, 2002), which resolves a subgrid-scale SIT distribution and uses an elastic–viscous–plastic rheology. Its resolution is about 2° in the Arctic Ocean. The CNRM-CM5.1 (Voldoire *et al.*, 2013) climate model includes the GELATO5 sea-ice model and its resolution is about 1° in the Arctic Ocean.

The EC-Earth version 2.1 and the EC-Earth version 2.3 climate models include the Louvain-la-Neuve version 2 Sea Ice Model (LIM2) (Fichefet and Morales Maqueda, 1997; Bouillon *et al.*, 2009). Its resolution is close to 1° in the Arctic Ocean.

The HadGEM1.2 sea-ice component shares much of its code with the CICE sea-ice model. The thermodynamic

representation of the sea ice includes a five-category SIT distribution scheme. The dynamic representation of the sea ice uses an elastic–viscous–plastic rheology. Its resolution is about 1° in the Arctic Ocean.

The CFSv2 includes the GFDL Sea Ice Simulator (Griffies *et al.*, 2004), which includes a SIT distribution with five categories and an elastic–viscous–plastic rheology.

References

Alexander MA, Bhatt US, Walsh J, Timlin M, Miller J. 2004. The atmospheric response to realistic Arctic sea ice anomalies in an AGCM during winter. *J. Clim.* **17**: 890–905.

Arfeuille GL, Mysak A, Tremblay LB. 2000. Simulation of the interannual variability in the wind-driven Arctic sea ice cover 1958–1988. *Clim. Dyn.* **16**: 107–121.

Årthun M, Eldevik T, Smedsrud LH, Skagseth Ø, Ingvaldsen RB. 2012. Quantifying the influence of Atlantic heat on Barents Sea ice variability and retreat. *J. Clim.* **25**: 4736–4743.

Balmaseda MA, Ferranti L, Molteni F, Palmer TN. 2010. Impact of 2007 and 2008 Arctic ice anomalies on the atmospheric circulation: Implications for long-rance predictions. *Q. J. R. Meteorol. Soc.* **136**: 1655–1664, doi: 10.1002/qj.661.

Balmaseda M, Mogensen K, Molteni F, Weaver A. 2012a. 'The NEMOVAR- COMBINE ocean reanalysis', COMBINE Technical report 1. http://www.combine-project.eu/Technical-Reports.1668.0.html (accessed 6 July 2014).

Balmaseda MA, Mogensen KS, Weaver AT. 2012b. Evaluation of the ECMWF ocean reanalysis ORAS4. *Q. J. R. Meteorol. Soc.* **139**: 1132–1161, doi: 10.1002/qj.2063.

Barnett DG. 1980. A long-range ice forecast method for the north coast of Alaska. In *Sea Ice Processes and Models*, Pritchard RS. (ed.): 360–372. University of Washington Press: Seattle, WA.

Belkin I, Levitus S, Antonov J, Malmberg SA. 1998. 'Great salinity anomalies' in the North Atlantic. *Prog. Oceanogr.* **41**: 1–68.

Bengtsson L, Semenov VA, Johannessen O. 2004. The early twentieth-century warming in the Arctic – A possible mechanism. *J. Clim.* **17**: 4045–4057.

Bitz CM, Lipscomb WH. 1999. An energy-conserving thermodynamic model of sea ice. *J. Geophys. Res.* **104**: 15,669–15,677, doi: 10.1029/1999JC900100.

Bitz CM, Roe GH. 2004. A mechanism for the high rate of sea-ice thinning in the Arctic Ocean. *J. Clim.* **17**: 3622–3631.

Bitz CM, Holland MM, Weaver AJ, Eby M. 2001. Simulating the ice-thickness distribution in a coupled climate model. *J. Geophys. Res.* **106**: 2441–2463, doi: 10.1029/1999JC000113.

Bitz CM, Holland MM, Hunke E, Moritz RE. 2005. Maintenance of the sea ice edge. *J. Clim.* **18**: 2903–2921.

Blanchard-Wrigglesworth E, Armour KC, Bitz CM, DeWeaver E. 2011a. Persistence and inherent predictability of Arctic sea ice in a GCM ensemble and observations. *J. Clim.* **24**: 231–250.

Blanchard-Wrigglesworth E, Bitz CM, Holland MM. 2011b. Influence of initial conditions and climate forcing on predicting Arctic sea ice. *Geophys. Res. Lett.* **38**: L18503, doi: 10.1029/2011GL048807.

Boer GJ. 2004. Long timescale potential predictability in an ensemble of coupled climate models. *Clim. Dyn.* **23**: 29–44.

Bouillon S, Morales Maqueda MA, Legat V, Fichefet T. 2009. An elastic viscous plastic sea ice model formulated on Arakawa B and C grids. *Ocean Modell.* **27**: 174–184, doi: 10.1016/j.ocemod.2009.01.004.

Briegleb BP, Bitz CM, Hunke EC, Lipscomb WH, Holland MM, Schramm JL, Moritz RE. 2004. 'Scientific description of the sea ice component in the Community Climate System Model version 3', NCAR Technical Note. NCAAR/TN-463+STR. National Center for Atmospheric Research: Boulder, CO.

Budyko M. 1969. The effect of solar radiation variations on the climate of the earth. *Tellus* **21**: 611–619.

Cardinali C. 2009. Monitoring the observation impact on the short-range forecast. *Q. J. R. Meteorol. Soc.* **135**: 239–250, doi: 10.1002/qj.366.

Cavalieri DJ, Parkinson C, Gloersen P, Zwally HJ. 1996. *Sea Ice Concentrations from Nimbus-7 SMMR and DMSP SSM/I-SSMIS Passive Microwave Data.* National Snow and Ice Data Center: Boulder, CO; digital media. http://nsidc.org/data/nsidc-0051.html (accessed 6 July 2014).

Caya A, Buehner M, Carrieres T. 2010. Analysis and forecasting of sea ice conditions with three-dimensional variational data assimilation and a coupled ice–ocean model. *J. Atmos. Oceanic Technol.* **27**: 353–369, doi: 10.1175/2009JTECHO701.1.

Chevallier M, Salas-Mélia D. 2012. The role of sea ice thickness distribution in the Arctic sea ice potential predictability: A diagnostic approach with a coupled GCM. *J. Clim.* **25**: 3025–3038.

Chevallier M, Salas-Mélia D, Voldoire A, Déqué M, Garric G. 2013. Seasonal forecasts of the pan-Arctic sea ice extent using a GCM-based seasonal prediction system. *J. Clim.* **26**: 6092–6104.

Chiang JCH, Biasutti M, Battisti DS. 2004. Sensitivity of the Atlantic ITCZ to conditions during the Last Glacial Maximum. *Paleoceanography* **18**: 1094, doi: 10.1029/2003PA000916.

Cohen J, Furtado JC, Barlow MA, Alexeev VA, Cherry JE. 2012. Arctic warming, increasing snow cover and widespread boreal winter cooling. *Environ. Res. Lett.* **7**: 014007, doi: 10.1088/1748-9326/7/1/014007.

Collins WD, Bitz CM, Blackmon ML, Bonan GB, Bretherton CS, Carton JA, Chang P, Doney SC, Hack JJ, Henderson TB, Kiehl JT, Large WG, McKenna DS, Santer BD, Smith RD. 2006. The Community Climate System Model version 3 (CCSM3). *J. Clim.* **19**: 2122–2143.

Day JJ, Tietsche S, Hawkins E. 2014. Pan-Arctic and Regional Sea Ice Predictability: Initialization Month Dependence. *J. Clim.* **27**: 4371–4390, doi: 10.1175/JCLI-D-13-00614.1.

Dee DP, Uppala SM, Simmons AJ, Berrisford P, Poli P, Kobayashi S, Andrae U, Balmaseda MA, Balsamo G, Bauer P, Bechtold P, Beljaars ACM, van de Berg L, Bidlot J, Bormann N, Delsol C, Dragani R, Fuentes M, Geer AJ, Haimberger L, Healy SB, Hersbach H, Hólm EV, Isaksen L, Kållberg P, Köhler M, Matricardi M, McNally AP, Monge-Sanz BM, Morcrette J-J, Park B-K, Peubey C, de Rosnay P, Tavolato C, Thépaut J-N, Vitart F. 2011. The ERA-interim reanalysis: Configuration and performance of the data assimilation system. *Q. J. R. Meteorol. Soc.* **137**: 553–597.

Deser C, Walsh JE, Timlin MS. 2000. Arctic sea ice variability in the context of recent atmospheric circulation trends. *J. Clim.* **13**: 617–633.

Deser C, Tomas R, Peng S. 2007. The transient atmospheric circulation response to North Atlantic SST and sea ice anomalies. *J. Clim.* **20**: 4751–4767.

Deser C, Tomas R, Alexander M, Lawrence D. 2010. The seasonal atmospheric response to projected Arctic sea ice loss in the late twenty-first century. *J. Clim.* **23**: 333–351.

Dickson RR, Meincke J, Malmberg SA, Lee AJ. 1988. The great salinity anomaly in the northern North Atlantic. 1968–1982. *Prog. Oceanogr.* **20**: 103–151.

Döscher R, Wyser K, Meier M, Qian M, Redler R. 2010. Quantifying Arctic contributions to climate predictability in a regional coupled ocean–ice–atmosphere model. *Clim. Dyn.* **34**: 1157–1176, doi: 10.1007/s00382-009-0567-y.

Drobot SD. 2007. Using remote sensing data to develop seasonal outlooks for Arctic regional sea ice minimum extent. *Remote Sens. Environ.* **111**: 137–147, doi: 10.1016/j.rse.2007.03.024.

Drobot SD, Maslanik JA. 2002. A practical method for long-range forecasting of ice severity in the Beaufort Sea. *Geophys. Res. Lett.* **29**: 1213, doi: 10.1029/2001GL014173.

Drobot SD, Maslanik JA, Fowler C. 2006. A long-range forecast of Arctic summer sea ice minimum extent. *Geophys. Res. Lett.* **33**: L10501, doi: 10.1029/2006GL026216.

Du H, Doblas-Reyes F, García-Serrano J, Guemas V, Soufflet Y, Wouters B. 2012. Sensitivity of decadal predictions to the initial atmospheric and oceanic perturbations. *Clim. Dyn.* **39**: 2013–2023, doi: 10.1007/s00382-011-1285-9.

Dulière V, Fichefet T. 2007. On the assimilation of ice velocity and concentration data into large-scale sea ice models. *Ocean Sci.* **3**: 321–335, doi: 10.5194/os-3-321-2007.

Eicken H. 2013. Ocean science: Arctic sea ice needs better forecasts. *Nature* **497**: 431–433, doi: 10.1038/497431a.

Escudier R, Mignot J, Swingedouw D. 2013. A 20-yr coupled ocean–sea ice–atmosphere variability mode in the North Atlantic in an AOGCM. *Clim. Dyn.* **40**: 619–636, doi: 10.1007/s00382-012-1402-4.

Evensen G. 1994. Sequential data assimilation with a nonlinear quasi-geostrophic model using Monte Carlo methods to forecast error statistics. *J. Geophys. Res.* **99**: 10143–10162, doi: 10.1029/94JC00572.

Fang Z, Wallace JM. 1994. Arctic sea ice variability on a timescales of weeks and its relation to atmospheric forcing. *J. Clim.* **7**: 1897–1913.

Fetterer F, Knowles K, Meier W, Savoie M. 2002. *Sea Ice Index*. National Snow and Ice Data Center: Boulder, CO. http://nsidc.org/data/nsidc-0051.html (accessed 6 July 2014).

Fichefet T, Morales Maqueda MA. 1997. Sensitivity of a global sea ice model to the treatment of ice thermodynamics and dynamics. *J. Geophys. Res.* **102**: 12609–12646, doi: 10.1029/97JC00480.

Francis JA, Vavrus SJ. 2012. Evidence linking Arctic amplification to extreme weather in mid-latitudes. *Geophys. Res. Lett.* **39**: L06801, doi: 10.1029/2012GL051000.

Francis JA, Chan W, Leathers DJ, Miller JR, Veron DE. 2009. Winter Northern Hemisphere weather patterns remember summer Arctic sea-ice extent. *Geophys. Res. Lett.* **36**: L07503, doi: 10.1029/2009GL037274.

Furevik T. 2001. Annual and interannual variability of Atlantic water temperatures in the Norwegian and Barents Seas 1980–1996. *Deep Sea Res.* **48A**: 383–404.

Gent PR, Danabasoglu G, Donner LJ, Holland MM, Hunke EC, Jayne SR, Lawrence DM, Neale RB, Rasch PJ, Vertenstein M, Worley PH, Yang Z-L, Zhang M. 2011. The Community Climate System Model version 4. *J. Clim.* **24**: 4973–4991, doi: 10.1175/2011JCLI4083.1.

Germe A, Chevallier M, Salas y Mélia D, Sanchez-Gomez E, Cassou C. 2014. Interannual predictability of Arctic sea ice in a global climate model: Regional contrasts and temporal evolution. *Clim. Dyn.*, doi: 10.1007/s00382-014-2071-2.

Gordienko PA. 1958. Arctic ice drift. In *Proceedings of the Conference on Arctic Sea Ice*, Thurson RW. (ed.). N.A.S. N.R.C. Publication No. 598: 210–220. NAS NRC: Washington, DC.

Goosse H, Holland M. 2005. Mechanisms of decadal Arctic variability in the Community Climate System Model CCSM2. *J. Clim.* **18**: 3552–3570.

Goosse H, Selten F, Haarsma R, Opstegh J. 2002. A mechanism of decadal variability of the sea ice volume in the northern hemisphere. *Clim. Dyn.* **19**: 61–83.

Goosse H, Selten F, Haarsma R, Opstegh J. 2003. Large sea ice volume anomalies simulated in a coupled climate model. *Clim. Dyn.* **20**: 523–536.

Goosse H, Arzel O, Bitz CM, de Montety A, Vancopennolle M. 2009. Increased variability of the Arctic summer ice extent in a warmer climate. *Geophys. Res. Lett.* **36**: L23702, doi: 101029/2009gl040546.

Griffies SM, Bryan K. 1997. Predictability of North Atlantic multidecadal climate variability. *Science* **275**: 181–184, doi: 10.1126/science.275.5297.181.

Griffies SM, Harrisson MJ, Pacanowski RC, Rosati A. 2004. 'Technical guide to MOM4', GFDL Ocean Group Technical Report 5. GFDL: Princeton, NJ. http://data1.gfdl.noaa.gov/~arl/pubrel/j/mom4beta/src/mom4/doc/guide.pdf (accessed 6 July 2014).

Gudkovich ZM. 1961a. Relation of the ice drift in the Arctic Basin to ice conditions in Soviet Arctic Seas. *Tr. Okeanogr. Kom. Akad. Nauk. SSSR* **11**: 14–21 (in Russian).

Gudkovich ZM. 1961b. On the nature of Pacific Currents in the Bering Strait and the causes of seasonal variations in their intensity. *Okeanologiya* **1**: 608–612 (in Russian).

Guemas V, Salas-Mélia D. 2008a. Simulation of the Atlantic meridional overturning circulation in an atmosphere–ocean global coupled model. Part I: A mechanism governing the variability of ocean convection in a preindustrial experiment. *Clim. Dyn.* **31**: 29–48, doi: 10.1007/s00382-007-0336-8.

Guemas V, Salas-Mélia D. 2008b. Simulation of the Atlantic meridional overturning circulation in an atmosphere-ocean global coupled model. Part II: A weakening in a climate change experiment: A feedback mechanism. *Clim. Dyn.* **30**: 831–844, doi: 10.1007/s00382-007-0328-8.

Guemas V, Salas-Mélia D, Kageyama M, Giordani H, Voldoire A, Sanchez-Gomez E. 2009. Winter interactions between weather regimes and marine surface in the North-Atlantic European region. *Geophys. Res. Lett.* **36**: L09816, doi: 10.1029/2009GL037551.

Guemas V, Doblas-Reyes FJ, Mogensen K, Tang Y, Keeley S. 2014. Ensemble of sea ice initial conditions for interannual climate predictions. *Clim. Dyn.* doi: 10.1007/s00382-014-2095-7.

Haak H, Jungclaus J, Mikolajewicz U, Latif M. 2003. Formation and propagation of great salinity anomalies. *Geophys. Res. Lett.* **30**: 1473–1476, doi: 10.1029/2003GL017065.

Hagedorn R, Doblas-Reyes FJ, Palmer TN. 2005. The rationale behind the success of multi-model ensembles in seasonal forecasting – I Basic concept. *Tellus* **57A**: 219–233.

Häkkinen S. 1999. A simulation of thermohaline effects of a great salinity anomaly. *J. Clim.* **6**: 1781–1795.

Hassol SJ. 2004. *Impacts of a Warming Arctic: Arctic Climate Impact Assessment.* Cambridge University Press: Cambridge, UK. http://www.amap.no/arctic-climate-impact-assessment-acia (accessed 6 July 2014).

Hawkins E, Tietsche S, Day JJ, Melia N, Haines K, Keeley S. 2014. Perspectives on the design of Arctic sea ice prediction systems. *Q. J. R. Meteorol. Soc.* (in this issue).

Hibler WD. 1979. A dynamic–thermodynamic sea ice model. *J. Phys. Oceanogr.* **9**: 815–846.

Hibler WD III 1986. Ice dynamics. *The Geophysics of Sea Ice*, *NATO ASI Series B* **146**, Untersteiner N. (ed.): 577–640. Plenum: New York, NY.

Hibler WD, Bryan K. 1987. A diagnostic ice-ocean model. *J. Phys. Oceanogr.* **17**: 987–1015.

Hilmer M, Jung T. 2000. Evidence for a recent change in the link between the North Atlantic Oscillation and Arctic sea ice export. *Geophys. Res. Lett.* **27**: 889–992, doi: 10.1029/1999GL010944.

Holland MM. 2003. The North Atlantic Oscillation–Arctic Oscillation in the CCSM2 and its influence on Arctic climate variability. *J. Clim.* **16**: 2767–2781.

Holland MM, Stroeve J. 2011. Changing seasonal sea ice predictor relationship in a changing Arctic climate. *Geophys. Res. Lett.* **38**: L18501, doi: 10.1029/2011GL049303.

Holland MM, Bitz CM, Eby M, Weaver AJ. 2001. The role of ice–ocean interactions in the variability of the North Atlantic thermohaline circulation. *J. Clim.* **14**: 656–675.

Holland MM, Bitz CM, Hunke EC, Lipscomb WH, Schramm JL. 2006. Influence of the sea ice thickness distribution on polar climate in CCSM3. *J. Clim.* **19**: 2398–2414.

Holland MM, Bitz CM, Tremblay B, Bailey DA. 2008. The role of natural versus forced change in future rapid summer Arctic ice loss. *Arctic Sea Ice Decline: Observations, Projections, Mechanisms and Implications*, *Geophysical Monograph Series* **180**: 133–150. American Geophysical Union: Washington, DC.

Holland MM, Bailey DA, Vavrus S. 2011. Inherent sea ice predictability in the rapidly changing Arctic environment of the Community Climate System Model version 3. *Clim. Dyn.* **36**: 1239–1253, doi: 10.1007/s00382-010-0792-4.

Honda M, Inoue J, Yamane S. 2009. Influence of low Arctic sea-ice minima on anomalously cold Eurasian winters. *Geophys. Res. Lett.* **36**: L08707, doi: 10.1029/2008GL037079.

Hunke EC, Dukowicz JK. 1997. An elastic–viscous–plastic model for sea ice dynamics. *J. Phys. Oceanogr.* **27**: 1849–1867.

Hunke EC, Lipscomb WH. 2004. '*CICE: The Los Alamos sea ice model, documentation and software*, version 3.1'. Technical report LA-CC-98-16. Los Alamos National Laboratory: Los Alamos, NM.

Ingram WJ, Wilson CA, Mitchell J. 1989. Modeling climate change: An assessment of sea ice and surface albedo feedbacks. *J. Geophys. Res.* **94**: 8609–8622, doi: 10.1029/JD094iD06p08609.

Ingvaldsen RB, Asplin L, Loeng H. 2004a. The seasonal cycle in the Atlantic transport to the Barents Sea during the years 1997–2001. *Cont. Shelf Res.* **24**: 1015–1032.

Ingvaldsen RB, Asplin L, Loeng H. 2004b. Velocity field of the western entrance to the Barents Sea. *J. Geophys. Res.* **109**: C03021, doi: 10.1029/2003JC001811.

Johnson CM, Lemke P, Barnett TP. 1985. Linear prediction of sea ice anomalies. *J. Geophys. Res.* **90**: 5665–5675, doi: 10.1029/JD090iD03p05665.

Johnson MA, Proshutinsky AY, Polyakov IV. 1999. Atmospheric patterns forcing two regimes of Arctic circulation: A return to anticyclonic conditions? *Geophys. Res. Lett.* **26**: 1621–1624, doi: 10.1029/1999GL900288.

Jungclaus JH, Koenigk T. 2010. Low-frequency variability of the Arctic climate: The role of oceanic and atmospheric heat transport variations. *Clim. Dyn.* **34**: 265–279.

Karklin VP. 1977. State and future of using of geliogeophysical factors for ice forecasts. *Probl. Arkt. Antarkt.* **50**: 45–48 (in Russian).

Krahmann G, Visbeck M. 2003. Arctic Ocean sea ice response to northern annular mode-like wind forcing. *Geophys. Res. Lett.* **30**: 1793, doi: 10.1029/2003GL017354.

Kiehl J, Gent P. 2004. The Community Climate System Model version 2. *J. Clim.* **17**: 3666–3682.

Knight RW. 1984. Introduction to a new sea-ice database. *Ann. Glaciol.* **5**: 81–84.

Koenigk T, Mikolajewicz U. 2009. Seasonal to interannual climate predictability in mid and high northern latitudes in a global coupled model. *Clim. Dyn.* **32**: 783–798, doi: 10.1007/s00382-008-0419-1.

Koenigk T, Mikolajewicz U, Haak U, Jungclaus J. 2006. Variability of Fram Strait sea ice export: Causes, impacts and feedbacks in a coupled climate model. *Clim. Dyn.* **26**: 17–34, doi: 10.1007/s00382-005-0060.1.

Koenigk T, Beattty C, Caian M, Döscher R, Wyser K. 2012. Potential decadal predictability and its sensitivity to sea ice albedo parameterization in a global coupled model. *Clim. Dyn.* **38**: 2389–2408, doi: 10.1007/s00382-011-1132-z.

Koenigk T, Brodeau L, Graversen RG, Karlsson J, Svensson G, Tjernström M, Willen U, Wyser K. 2013. Arctic climate change in 21st century CMIP5 simulations with EC-Earth. *Clim. Dyn.* **40**: 2719–2743, doi: 10.1007/s00382-012-1505-y.

Kumar A, Perlwitz J, Eischeid J, Quan X, Xu T, Zhang T, Hoerling M, Jha B, Wang W. 2010. Contribution of sea ice loss to Arctic amplification. *Geophys. Res. Lett.* **37**: L21701, doi: 10.1029/2010GL045022.

Kwok R. 2000. Recent changes in the Arctic sea ice motion associated with the North Atlantic Oscillation. *Geophys. Res. Lett.* **27**: 775–778, doi: 10.1029/2010GL045022.

Kwok R. 2009. Outflow of Arctic Ocean sea ice into the Greenland and Barents Seas: 1979–2007. *J. Clim.* **22**: 2438–2457, doi: 10.1175/2008JCLI2819.1.

Kwok R, Rothrock DA. 1999.Variability of Fram Strait flux and North Atlantic Oscillation. *J. Geophys. Res.* **104**: 5177–5189, doi: 10.1029/1998JC900103.

Kwok R, Rothrock DA. 2009. Decline in Arctic sea ice thickness from submarine and IceSat records: 1958–2008. *Geophys. Res. Lett.* **36**: L15501, doi: 10.1029/2009gl039035.

Kwok R, Spreen G, Pang S. 2013. Arctic sea ice circulation and drift speed: Decadal trends and ocean currents. *J. Geophys. Res. Oceans* **118**: 2408–2425, doi: 10.1002/jgrc.20191.

L'Hévéder B, Houssais MN. 2001. Investigating the variability of the Arctic sea ice thickness in response to a stochastic thermodynamic atmospheric forcing. *Clim. Dyn.* **17**: 107–125.

Lindsay R. 2010. New unified sea ice thickness climate data record. *Eos Trans. Am. Geophys. Union* **91**: 405–406.

Lindsay RW, Zhang J. 2006. Assimilation of ice concentration in an ice–ocean model. *J. Atmos. Oceanic Technol.* **23**: 742–749.

Lindsay RW, Zhang J, Schweiger AJ, Steele MA. 2008. Seasonal predictions of ice extent in the Arctic Ocean. *J. Geophys. Res.* **113**: C02023, doi: 10.1029/2007jc004259.

Lipscomb WH. 2001. Remapping the thickness distribution in sea ice models. *J. Geophys. Res.* **106**: 13989–14000, doi: 10.1029/2000JC000518.

Lisaeter KA, Rosanova J, Evensen G. 2003. Assimilation of ice concentration in coupled ice–ocean model, using the Ensemble Kalman filter. *Ocean Dyn.* **53**: 368–388, doi: 10.1007/s10236-003-0049-4.

Liu J, Curry JA, Wang H, Song M, Horton RM. 2012. Impact of declining Arctic sea ice on winter snowfall. *Proc. Natl. Acad. Sci. U.S.A.* **109**: 4074–4079, doi: 10.1073/pnas.1114910109.

Lukovich JV, Barber DG. 2007. On the spatiotemporal behavior of sea ice concentration anomalies in the Northern Hemisphere. *J. Geophys. Res.* **112**: D13117, doi: 10.1029/2006JD007836.

Magnusdottir G, Deser C, Saravanan R. 2004. The effects of North Atlantic SST and sea ice anomalies on the winter circulation in CCM3. Part I: Main features and storm track characteristics of the response. *J. Clim.* **17**: 857–876.

Manabe S, Stouffer RJ. 1980. Sensitivity of a global climate model to an increase of CO_2 concentration in the atmosphere. *J. Geophys. Res.* **85**: 5529–5554, doi: 10.1029/JC085iC10p05529.

Marsland S, Haak H, Jungclaus J, Latif M, Roeske F. 2003. The Max-Planck Institut global ocean/sea-ice model with orthogonal curvilinear coordinates. *Ocean Modell.* **5**: 91–127.

Mauritsen T, Stevens B, Roeckner E, Crueger T, Esch M, Giorgetta M, Haak H, Jungclaus J, Klocke D, Matei D, Mikolajewicz U, Notz D, Pincus R, Schmidt H, Tomassini L. 2012. Tuning the climate of a global model. *J. Adv. Model. Earth Syst.* **4**: M00A01, doi: 10.1029/2012MS000154.

Maykut GA. 1982. Large-scale heat exchange and ice production in the central Arctic. *J. Geophys. Res.* **87**: 7971–7984, doi: 10.1029/JC087iC10p07971.

Merryfield WJ, Lee WS, Boer GJ, Kharin VV, Scinocca JF, Flato CM, Ajayamohan RS, Fyfe JC, Peng Y, Palavarapu S. 2013a. The Canadian seasonal to interannual prediction system. Part I: Models and initialization. *Mon. Weather Rev.* **141**: 2910–2945, doi: 10.1175/MWR-D-12-00216.1.

Merryfield WJ, Lee WS, Wang W, Chen M, Kumar A. 2013b. Multi-system seasonal predictions of Arctic sea ice. *Geophys. Res. Lett.* **40**: 1551–1556, doi: 10.1002/grl.50317.

Mikolajewicz U, Sein DV, Jacob D, Koenigk T, Podzun T, Semmler T. 2005. Simulating Arctic sea ice variability with a coupled regional atmosphere–ocean–sea ice model. *Meteorol. Z.* **14**: 793–800, doi: 10.1127/0941-2948/2005/0083.

Min SK, Zhang X, Zwiers FW, Agnew T. 2008. Human influence on the Arctic sea ice detectable from early 1990s onwards. *Geophys. Res. Lett.* **35**: L21701, doi: 10.1029/2008GL035725.

Mogensen KS, Balmaseda MA, Weaver A. 2011. The NEMOVAR Ocean Data Assimilation as Implemented in the ECMWF Ocean Analysis for System 4, *ECMWF Technical Memorandum* 668. ECMWF: Reading, UK.

Mysak L, Venegas S. 1998. Decadal climate oscillations in the Arctic: A new feedback loop for atmosphere–ice–ocean interactions. *Geophys. Res. Lett.* **25**: 3607–3610, doi: 10.1029/98GL02782.

Mysak L, Manak DA, Marsden RF. 1990. Sea ice anomalies observed in the Greenland and Labrador Seas during 1901–1984 and their relation to an interdecadal Arctic climate cycle. *Clim. Dyn.* **5**: 111–133.

Notz D, Marotzke J. 2012. Observations reveal external driver for Arctic sea-ice retreat. *Geophys. Res. Lett.* **39**: L08502, doi: 10.1029/2012GL051094.

Ogi M, Yamazaki K, Wallace JM. 2010. Influence of winter and summer surface wind anomalies on summer Arctic sea ice extent. *Geophys. Res. Lett.* **37**: L07701, doi: 10.1029/2009GL042356.

Partington K, Flynn T, Lamb D, Bertoia C, Dedrick K. 2003. Late twentieth century Northern Hemisphere sea-ice record from U.S. National Ice Center ice charts. *J. Geophys. Res.* **108**: 3343, doi: 10.1029/2002JC001623.

Petoukhov V, Semenov VA. 2010. A link between reduced Barents–Kara sea ice and cold winter extremes over northern continents. *J. Geophys. Res.* **115**: D21111, doi: 10.1029/2009JD013568.

Polyakov IV, Proshutinsky AY, Johnson MA. 1999 Seasonal cycles in two regimes of the Arctic climate. *J. Geophys. Res.* **104**: 25761–25788, doi: 10.1029/1999JC900208.

Proshutinsky AY. 1993. *The Arctic Ocean Level Oscillations.* Gidrometeoizdat: St Petersburg, Russia (in Russian).

Proshutinsky AY. 1988. Modeling seasonal fluctuations of the level of the Arctic Ocean. *Sov. Meteorol. Hydrol.* **2**: 57–65 (English Translation).

Proshutinsky A, Johnson MA. 1997. Two circulation regimes of the wind-driven Arctic Ocean. *J. Geophys. Res.* **102**: 12493–12514, doi: 10.1029/97JC00738.

Rayner NA, Parker DE, Horton EB, Folland CK, Alexander LV, Rowell DP, Kent EC, Kaplan A. 2003. Global analyses of sea surface temperature, sea ice and night marine air temperature since the late nineteenth century. *J. Geophys. Res.* **108**: 4407, doi: 10.1029/2002JD002670.

Rigor IG, Wallace JM, Colony RL. 2002. Response of sea ice to the Arctic Oscillation. *J. Clim.* **15**: 2648–2663.

Roeckner E, Baeuml G, Bonaventura L, Brokopf R, Esch M, Giorgetta M, Hagemann S, Kirchner I, Kornblueh L, Manzini E, Rhodin A, Schlese U, Schulzweida U, Tompkins A. 2003. 'The atmosphere general circulation model ECHAM5 part I: Model description', MPI Report 349. *Max-Planck Institut für Meteorology*: Hamburgh, Germany, p. 127.

Rudels B, Anderson LG, Jones EP. 1996. Formation and evolution of the surface mixed layer and halocline of the Arctic Ocean. *J. Geophys. Res.* **101**: 8807–8821, doi: 10.1029/96JC00143.

Saha S, Moorthi S, Pan H-L, Wu X, Wang J, Nadiga S, Tripp P, Kistler R, Woollen J, Behringer D, Liu H, Stokes D, Grumbine R, Gayno G, Wang J, Hou Y-T, Chuang H-Y, Juang H-MH, Sela J, Iredell M, Treadon R, Kleist D, Van Delst P, Keyser D, Derber J, Ek M, Meng J, Wei H, Yang R, Lord S, Van Den Dool H, Kumar A, Wang W, Long C, Chelliah M, Xue Y, Huang B, Schemm J-K, Ebisuzaki W, Lin R, Xie P, Chen M, Zhou S, Higgins W, Zou C-Z, Liu Q, Chen Y, Han Y, Cucurull L, Reynolds RW, Rutledge G, Goldberg M. 2010. The NCEP climate forecast system reanalysis. *Bull. Am. Meteorol. Soc.* **91**: 1015–1057.

Salas-Mélia D. 2002. A global coupled sea ice/ocean model. *Ocean Modell.* **4**: 137–172.

Salas-Melia D, Chauvin F, Deque M, Douville H, Gueremy JF, Marquet P, Planton S, Royer JF, Tyteca S. 2005. 'Description and validation of the CNRM-CM3 global coupled model', *CNRM Technical report* 103. CNRM/GMGEC: Toulouse, France.

Schauer U, Loeng H, Rudels B, Ozhigin VK, Dieck W. 2002. Atlantic water flow through the Barents and Kara Seas. *Deep Sea Res.* **49A**: 2281–2298.

Schlichtholz P. 2011. Influence of oceanic heat variability on sea ice anomalies in the Nordic Seas. *Geophys. Res. Lett.* **38**: L05705, doi: 10.1029/2010GL045894.

Schmith T, Hansen C. 2003. Fram Strait ice export during the 19th and 20th centuries: Evidence for multidecadal variability. *J. Clim.* **16**: 2782–2791.

Schweiger A, Lindsay R, Zhang J, Steele M, Stern H, Kwok R. 2011. Uncertainty in modeled Arctic sea ice volume. *J. Geophys. Res.* **116**: C00D06, doi: 10.1029/2011JC007084.

Screen JA, Simmonds I. 2010. The central role of diminishing sea ice in recent Arctic temperature amplification. *Nature* **464**: 1334–1337, doi: 10.1038/nature09051.

Screen JA, Simmonds I, Deser C, Tomas R. 2013. The atmospheric response to three decades of observed Arctic sea ice loss. *J. Clim.* **26**: 1230–1248.

Semtner AJ. 1987. A numerical study of sea ice and ocean circulation in the Arctic. *J. Phys. Oceanogr.* **17**: 1077–1099.

Serreze MC, Maslanik JA, Barry RG, Demaria TL. 1992. Winter atmospheric circulation in the Arctic Basin and possible relationships to the Great Salinity Anomaly in the northern North Atlantic. *Geophys. Res. Lett.* **19**: 293–296, doi: 10.1029/91GL02946.

Serreze MC, Holland MM, Stroeve JC. 2007. Perspectives on the Arctic's shrinking sea-ice cover. *Science* **315**: 1533–1536.

Serreze MC, Barnett AP, Stroeve JC, Kindig N, Holland MM. 2009. The emergence of surface-based Arctic amplification. *Cryosphere* **3**: 11–19.

Sigmond M, Fyfe JC, Flato GM, Kharin VV, Merryfield WJ. 2013. Seasonal forecast skill of Arctic sea ice area in a dyamical forecast system. *Geophys. Res. Lett.* **40**: 529–534, doi: 10.1002/grl.50129.

Smith LC, Stephenson SR. 2013. New Trans-Arctic shipping routes navigable by midcentury. *Proc. Natl. Acad. Sci. U.S.A.* **110**: 4871–4872, doi: 10.1073/pnas.1214212110.

Smith LM, Miller GH, Otto-Bliesner B, Shin SI. 2003. Sensitivity of the Northern Hemisphere climate system to extreme changes in Holocene Arctic sea ice. *Quat. Sci. Rev.* **22**: 645–658.

Sokolov AL. 1962. Drift of ice in the Arctic Basin and changes in ice conditions over the northern sea route. *Probl. Arct. Antarct.* (English Translation) **11**: j1–j20.

Solomon S, Qin D, Manning M, Marquis M, Averyt K, Tignor MMB, Miller HL, Chen Z. (eds.) 2007. *Climate Change 2007: The Physical Science Basis.* Cambridge University Press: Cambridge, UK.

Steele M, Morison J. 1993. Hydrography and vertical fluxes of heat and salt northeast of Svalbard in autumn. *J. Geophys. Res.* **98**: 10013–10024, doi: 10.1029/93JC00937.

Steele M, Ermold W, Zhang J. 2008. Arctic ocean surface warming trends over the past 100 years. *Geophys. Res. Lett.* **35**: L02614, doi: 10.1029/2007GL031651.

Stroeve JC, Serreze MC, Holland MM, Kay JE, Malanik J, Barrett AP. 2012. The Arctic's rapidly shrinking sea ice cover: A research synthesis. *Clim. Change* **110**: 1005–1027.

Strong C. 2012. Atmospheric influence on Arctic Marginal Ice position and width in the Atlantic Sector, February–April 1979–2010. *Clim. Dyn.* **39**: 3091–3102, doi: 10.1007/s00382-012-1356-6.

Thorndike AS, Rothrock D, Maykut GA, Colony R. 1975. The thickness distribution of sea ice. *J. Geophys. Res.* **80**: 4501–4513, doi: 10.1029/JC080i033p04501.

Tietsche S, Notz D, Jungclaus JH, Marotzke J. 2013a. Predictability of large interannual Arctic sea-ice anomalies. *Clim. Dyn.* **41**: 2511–2526, doi: 10.1007/s00382-013-1698-8.

Tietsche S, Notz D, Jungclaus JH, Marotzke J. 2013b. Assimilation of sea ice concentration in a global climate model – Physical and statistical aspects. *Ocean Sci.* **9**: 19–36, doi: 10.5194/os-9-19-2013.

Tietsche S, Day JJ, Guemas V, Hurlin WJ, Keeley SPE, Matei D, Msadek R, Collins M, Hawkins E. 2014. Seasonal to interannual Arctic sea-ice predictability in current global climate models. *Geophys. Res. Lett.* **41**: 1035–1043, doi: 10.1002/2013GL058755.

Tivy A, Alt B, Howell SEL, Wilson K, Yackel J. 2007. Long-range prediction of the shipping season in Hudson Bay: A statistical approach. *Weather and Forecasting* **22**: 1063–1075.

Tsukernik M, Deser C, Alexander M, Tomas R. 2009. Atmospheric forcing of Fram Strait sea ice export: A closer look. *Clim. Dyn.* **35**: 1349–1360, doi: 10.1007/s003-82-009-0647-z.

Ukita J, Honda M, Nakamura H, Tachibana Y, Cavlieri DJ, Parkinson CL, Koide H, Yamamoto K. 2007. Northern Hemisphere sea ice variability: Lag structure and its implications. *Tellus Ser. A* **59**: 261–272, doi: 10.111/j1600-08702006.00223.

Venegas S, Mysak L. 2000. Is there a dominant timescale of natural climate variability in the Arctic? *J. Clim.* **13**: 3413–3434.

Vinje T. 2001a. Anomalies and trends of sea ice extent and atmospheric circulation in the Nordic Seas during the period 1864–1998. *J. Clim.* **14**: 255–267.

Vinje T. 2001b. Fram Strait ice fluxes and atmospheric circulation: 1950–2000. *J. Clim.* **14**: 3508–3517.

Voldoire A, Sanchez-Gomez E, Salas y Mélia D, Decharme B, Cassou C, Sénési S, Valcke S, Beau I, Alias A, Chevallier M, Déqué M, Deshayes J, Douville H, Fernandez E, Madec G, Maisonnave E, Moine M-P, Planton S, Saint-Martin D, Szopa S, Tyteca S, Alkama R, Belamari S, Braun A, Coquart L, Chauvin F. 2013. The CNRM-CM5.1 global dynamical model: Description and basic evaluation. *Clim. Dyn.* **40**: 2091–2121, doi: 10.1007/s00382-011-1259-y.

Wadhams P. 1981. The ice cover in the Greenland and Norwegian Seas. *Rev. Geophys.* **19**: 345–393.

Wang W, Chen M, Kumar A. 2013. Seasonal prediction of Arctic sea ice extent from a coupled dynamical forecast system. *Mon. Weather Rev.* **141**: 1375–1394.

Walsh JE. 1980. Empirical orthogonal function and the statistical predictability of sea ice extent. In *Sea Ice Processes and Models*, Pritchard RS. (ed.): 373–384 .University of Washington Press: Seattle, WA.

Walsh JE. 1983. The role of sea ice in climatic variability: Theories and evidence. *Atmos. Ocean* **21**: 229–242.

Walsh JE, Chapman WL. 1990. Arctic contribution to upper-ocean variability in the North Atlantic. *J. Clim.* **3**: 1462–1473.

Walsh JE, Johnson CM. 1979. An analysis of Arctic sea ice fluctuations. *J. Phys. Oceanogr.* **9**: 580–591.

Winton M. 2003. On the climatic impact of ocean circulation. *J. Clim.* **16**: 2875–2889.

Wohlleben TMH, Weaver AJ. 1995. Interdecadal climate variability in the subpolar North Atlantic. *Clim. Dyn.* **11**: 459–467.

Woodgate RA, Weingartner T, Lindsay R. 2010. The 2007 Bering Strait oceanic heat flux and anomalous Arctic sea-ice retreat. *Geophys. Res. Lett.* **37**: L01602, doi: 10.1029/2009GL041621.

Wu B, Wang J, Walsh JE. 2006. Dipole anomaly in the winter Arctic atmosphere and its association with Arctic sea ice motion. *J. Clim.* **19**: 210–225, doi: 10.1175/JCLI3619.1.

Yang S, Christensen JH. 2012. Arctic sea ice reduction and European cold winters in CMIP5 climate change experiments. *Geophys. Res. Lett.* **39**: L20707, doi: 10.1029/2012GL053338.

Yang J, Neelin JD. 1997. Decadal variability in coupled sea ice thermohaline circulation systems. *J. Clim.* **10**: 3059–3076.

Zhang J, Rothrock DA. 2001. A thickness and enthalpy distribution sea ice model. *J. Phys. Oceanogr.* **31**: 2986–3001.

Zhang J, Rothrock DA. 2003. Modelling global sea ice with a thickness and enthalpy distribution model in generalized curvilinear coordinates. *Mon. Weather Rev.* **131**: 681–697.

Zhang J, Thomas D, Rothrock DA, Lindsay RW, Yu Y, Kwok R. 2003. Assimilation of ice motion observations and comparisons with submarine ice thickness data. *J. Geophys. Res.* **108**: 3170, doi: 10.1029/2001JC001041.

Zhang J, Steele M, Rothrock DA, Lindsay RW. 2004. Increasing exchanges of Greenland–Scotland ridge and their links with the North Atlantic Oscillation and Arctic sea ice. *Geophys. Res. Lett.* **31**: L09307, doi: 10.1029/2003GL019304.

Zhang J, Steele M, Lindsay R, Schweiger A, Morison J. 2008. Ensemble 1-year predictions of Arctic sea ice for the spring and summer of 2008. *Geophys. Res. Lett.* **35**: L08502, doi: 10.1029/2008GL033244.

